الجمهورية الجزائرية الديمقراطية الشعبية

People's Democratic Republic of Algeria

وزارة التعليم العالي والبحث العلمي

Ministry of Higher Education and Scientific Research

المدرسة العليا لأساتذة التعليم التكنولوجي –سكيكدة–

Higher Normal School of Technological Education –Skikda-

Department of Physics and Chemistry قسم الفيزياء و الكيمياء

مذكرة التخرج

Graduation thesis

لنيل شهادة أستاذ تعليم ثانوي

Presented to obtain the degree of secondary school teacher

Entitled

TCO-Silicon solar cells simulation by Afors-Het software

Presented by

Haridi Heythem

Jury members

Dr. Bedboudi Hayette	**MCA**	**ENSET SKIKDA**	**PRESIDENT**
Dr. Benredouane Rabab	**MCB**	**ENSET SKIKDA**	**SUPERVISOR**
Dr. Nemiri Ouarda	**MCA**	**ENSET SKIKDA**	**EXAMINER**
Dr. Mokhnech Chafia	**MCB**	**ENSET SKIKDA**	**EXAMINER**

June 2024 جوان

DEDICATIONS

For me because I needed to write this.

For my father NOURREDINE, who tries his very best not to be his worst.

And for my mother FARIDA, even though you are no longer here with me, I can still feel your love guiding me, you are always in my heart I love you and miss you dearly.

For my sisters, who are the halves of the sun that warms me.

For you, if any part of this thesis helps you feel a little more understood.

For all my friends and colleagues with whom I shared the university life with its lights and shadows, namely: Ahmed, Charaf, Manef, Tarek, Aymen, Ali, Silouma, Mohamed-amine, El-Hareth, Souhaib, Saif, Djalal, my pool friends, my tif friends...

HEYTHEM ^^

ACKNOWLEDGEMENT

I would like to thank God, for letting me through all the difficulties. I have experienced your guidance day by day You are the one who let me finish my degree.

I would like to acknowledge and give my warmest thanks to my supervisor Dr Ben Redouane Rabab who made this work possible. Her guidance and advice carried me through all the stages of writing project.

I would like also to express my special thanks to the members of the jury who would examine and evaluate this research.

I thank all the staff of Enset Skikda for their cooperation and kind support throughout my research period.

Finally, I would like to thank all those who have contributed to the success of this thesis.

TABLE OF CONTENTS

Chapter II: Solar cell

Chapter III: simulation, results and discussion

LIST OF FIGURES

LIST OF TABLES

LIST OF SYMBOLS

Symbol	Physical quantities
E_g	Energy gap.
E_F	Fermi level.
E_c	Energy level of conduction band.
K	Boltzmann's constant.
T	Temperature.
N_C	Number of electrons in conduction band.
N_D	Concentration of donor impurity.
E_V	Energy level of valence band.
N_V	Number of electrons in valence band.
N_A	Concentration of acceptor impurity.
I	The net current flowing through the diode.
AM	Air mass.
S	The intensity of direct solar irradiance.
I_{SC}	Short-circuit current.
V_{OC}	Open-circuit voltage.
mpp	Maximum power point.
FF	Fill factor.

P_{SUN}	Power of sunlight.
R_P	Shunt resistance.
R_S	Series resistance.
η	Efficiency.
$\boldsymbol{n}$	The product of refractive index.
d	Layer thickness.
Φ_m	Work function of the metal.
Φ_s	Work function of semiconductor.
$q\Phi_b$	Potential barrier.
μ	Electron mobility.
TCOs	Transparent conducting oxides.

GENERAL INTRODUCTION

The search for renewable and non-polluting energy sources is one of the major technological challenges of the twenty-first century. In addition, given the gradual depletion of fossil energy reserves, the growing environmental problems associated with the use of these energies, and the rising operating costs.

Therefore, the solution to these problems lies in the mastery of renewable energies and especially the photovoltaic conversion solar energy which is inexhaustible and clean and occupies a leading place. This form of energy is a direct transformation of solar energy into electric energy. It is essentially provided by silicon solar cells and the manufacture of them is increasingly controlled.

A silicon solar cell is the most common type of solar cells, accounting for roughly 95% of the photovoltaic market. It utilizes silicon, the second-most abundant element on Earth after oxygen, to convert sunlight into electricity.

The main factor still holding back the massive use of this clean energy production process is the manufacturing costs deemed excessive in relation to fossil or nuclear energy. For this, the challenge facing the photovoltaic industry is to increase the physical/economic performance ratio of solar cells, through the introduction of technological means to improve conversion efficiency, using new materials and structures that can increase the performance of solar devices, while the reduce of manufacturing costs through easy and inexpensive implementation techniques.

In this context, we have been interested in the study of titanium dioxide (TiO_2) to optimize the performance of the photovoltaic cell with heterojunction from a silicon substrate and a thin layer TiO_2 emitter.

TiO_2 is a semiconductor material, it is part of the TCO (transparent conducting oxide) which are semi-conductors with large gap. TCOs are very promising in the framework of the realization of solar cells., according to their good electrical conductivity and their excellent optical transparency in the field of visible and near infrared. In this work, we study the zinc oxide, which is also belongs to the TCOs. For this reason, we discuss the effect of using the

TiO_2(n) and ZnO(n) semiconductors as a transparent conductive oxide (TCO) on electric properties of the TiO_2(n)-c-Si(p) and ZnO(n)-c-Si(p) solar cell by using the AFORS-HET simulation software [1].

To complete our work, we have structured this memory into three chapters:

We divide the first chapter into two main sections, in the first section, we give some details about semiconductors and their most important properties: their types, the p-n junction and their applications. We also give the classification of materials according to their electric properties. In the second section, we study the solar radiation, we present some notions related to it: how it reached the earth, measured its intensity and its different properties.

In the second chapter, we mention the components of the solar cells, their function process, their different characteristics and all their types. We conclude this chapter with some concepts of Transparent conducting oxides (TCOs), specifically titanium dioxide.

The final chapter focuses on the simulation of the TiO_2(n)-c-Si(p) and the ZnO(n)-c-Si(p) solar cells.

For this, we use the software AFORES-HET [1] (Automate for Simulation of Heterostructures). Finally, we discuss and interpretation of the simulation results.

CHAPTER I
SEMI-CONDUCTORS AND SOLAR RADIATION

I-1 INTRODUCTION:

Using the sun's power is made possible by semiconductors, which are the workhorses of modern electronics. Their unique ability to control conductivity makes them ideal partners for solar radiation. When sunlight, packed with energy particles called photons, strikes a semiconductor, it excites electrons within the material. This causes a flow of electricity, known as the photovoltaic effect.

Solar cells, built with specific semiconductors and a p-n junction, transforms the sunlight into clean and renewable energy.

I-2 SEMI-CONDUCTORS:

Materials with conductivity between non-conductors or insulators (like most ceramics) and conductors (usually metals) are known as semiconductors. Semiconductors can be compounds like cadmium selenide or gallium arsenide or pure elements like germanium or silicon. Doping is the technique of adding tiny amounts of impurities to pure semiconductors, which significantly alters the material's conductivity. Semiconductors play a significant role in the creation of electronic gadgets, which makes them indispensable to our daily existence. Consider a world without electronics, there wouldn't be any computers, TVs, radios, video games, or subpar medical diagnosis tools.

I-2-1 CLASSIFICATION OF MATERIALS:

Materials can be classified based on their resistivity which is the flip side of the coin when it comes to electrical conductivity While conductivity tells you how easily a material conducts electricity, resistivity tells you how much it resists that flow.

Based on their resistivity, materials can be broadly categorized into three main groups:

I-2-1-1 CONDUCTORS:

The materials with the lowest resistivity at room temperature, typically less than 10^{-3} Ω.cm, are conductors as gold, silver and carbon… (figure I-1). Electrical conduction is mainly carried out by free electrons whose concentration differs little from one conductor to another, regardless of its purity. An increase in temperature causes a slight increase in resistivity, which can be explained by the fact that free electrons are hampered in their movement by the vibrations (increasing with temperature) of the atoms [2].

I-2-1-2 INSULATORS:

Materials with a resistivity typically greater than 10^6 Ω.cm are considered insulators (figure I-1); this is the case for Glass, Quartz, Silica (SiO_2), and Carbon (diamond). This time, the increase in temperature can cause the release of electrons (as well as holes) that can participate in electrical conductivity, causing a decrease in resistance with temperature [2].

I-2-1-3 SEMICONDUCTORS:

Between metals and insulators are semiconductors (SC) with resistivity ranging from 10^{-3} to 10^6 Ω.cm (figure I-1). Electrical conduction is done by electrons and holes. A semiconductor can be either pure, in which case it is called "intrinsic," or doped by impurities (which allow to control its resistivity), in which instance it is called "extrinsic." If we take, for example, sufficiently pure silicon and add one atom of boron or phosphorus to 10^5 silicon atoms, its resistance will pass from 10^3 to approximately 10^{-2} Ω.cm[2].

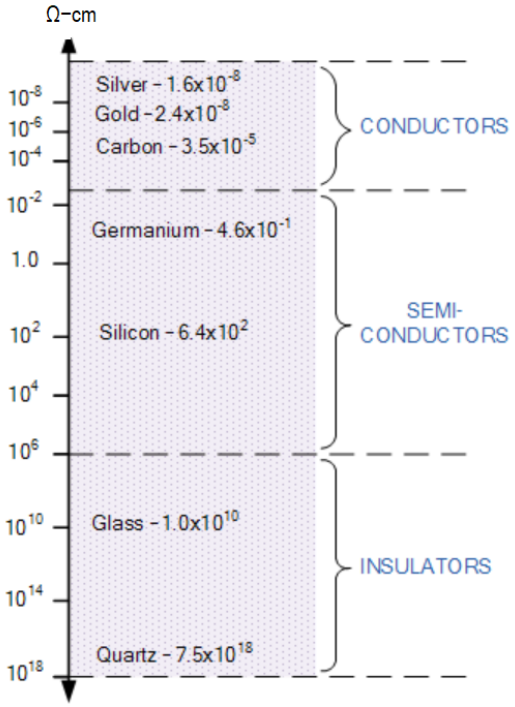

Figure (I-1): Classification of materials on basis of resistivity.

I-2-2 ENERGY BANDS:

Electron energies at our disposal enable us to distinguish between semiconductors, conductors, and insulators (figure I-2). Discrete energy levels exist in free atoms, but the available energy states in solid materials (insulators, semiconductors, and conductors) are so close to each other that they form bands. The band gap represents an energy range devoid of electronic states. In semiconductors, the gap between the valence and conduction bands is small enough to allow thermal excitation of electrons from the valence to the conduction band. For Germanium, the forbidden gap is 0.72 eV, and for Silicon, it is 1.1 eV. Thus, semiconductors require small conductivity. In insulators, the valence band and conduction band are separated by a large gap, whereas in good conductors like metals, the valence band overlaps the conduction band [3].

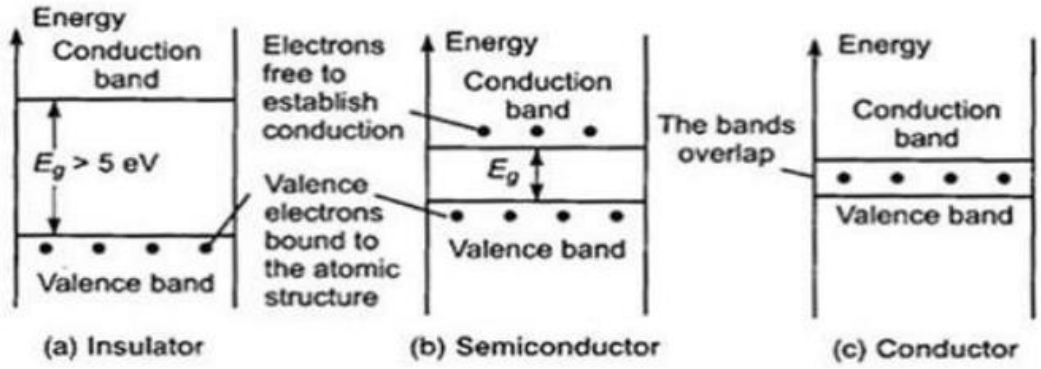

Figure (I-2): Energy band diagram of insulator, semi-conductor and conductor [3].

I-2-3 TYPES OF SEMI-CONDUCTORS:

We can classify semi-conductors in two types: intrinsic and extrinsic. There are many differences between them as we mention in table I-1.

I-2-3-1 INTRINSIC (PURE) SEMI-CONDUCTORS:

In the silicon semiconductor we have only the silicon atoms (figure I-3). These atoms have a valence of 4 and an atomic number of 14. At zero Kelvin, no electron is available for conduction, and all silicon atoms form covalent bonds with their nearby Si atoms.

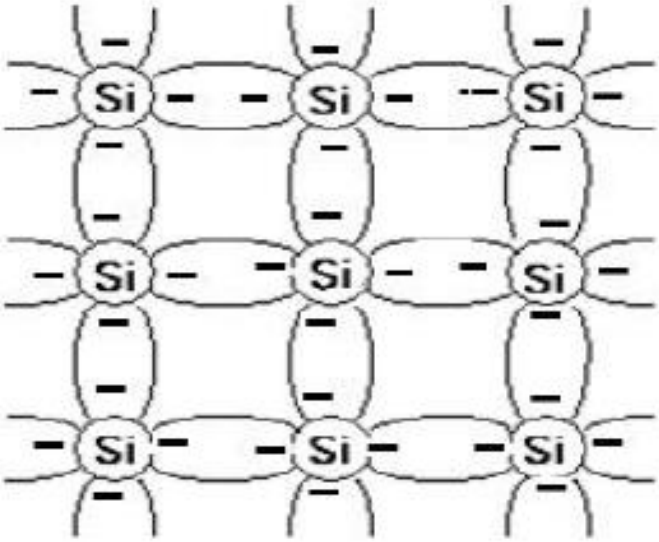

Figure (I-3): The schematic of an intrinsic Silicon semi-conductor [4].

As a result, pure silicon functions as an insulator at absolute 0 K. These covalent bonds break, and some electrons are released as the temperature rises above 0 K. These free-moving electrons within the crystal are what give it its conductivity. So, they are called free electrons.

An empty space known as a hole, which also serves as a current carrier, is left behind by each electron. Current is made up of these electrons and holes, which travel in opposing directions due to an external force [4].

I-2-3-2 EXTRINSIC SEMICONDUCTORS:

Impurities are given to pure semiconductors to boost their conductivity. We refer to this procedure as doping. The available energy levels in semiconductors change when impurities are added. The band structure shows the appearance of one or more energy levels [4].

An extrinsic semiconductor is classified as n-type if the majority of its charge carriers are conduction electrons, and p-type if the majority of its charge carriers are holes.

Table I-1: differences between intrinsic and extrinsic semi-conductors [5].

	Intrinsic semi-conductors	**Extrinsic semi-conductors**
Doping	no deliberate addition of impurity atoms.	purposeful doping implantation of impurity atoms.
Type of atoms	composed of only one kind of atom.	doped with specific impurity atoms: P-type ⟶ trivalent N-type ⟶ pentavalent.
Charge carriers	almost equal amounts of holes and electrons.	The dominant charge carriers are determined by the type of doping.
Conductivity type	exhibits both n-type and p-type conductivity.	Exhibits n-type or p-type conductivity based on doping.
Majority charge carriers	Electrons and holes share similar concentrations.	The majority of carriers can be electrons (n-type) or holes (p-type).
Electrical conductivity	comparatively low electrical conductivity.	Increased electrical conductivity due to intentional doping.
Energy levels	The valence and conduction bands stay in close proximity.	Doping modifies energy levels to widen the bandgap.
Bandgap modification	The bandgap doesn't change all that much.	Based on the kind and amount of dopants, bandgap can be changed.
Applications	Not frequently utilised for practical devices.	utilised widely in electronic devices such as diodes and transistors.

I-2-4 DOPING:

I-2-4-1 P-TYPE MATERIAL:

P-type materials are created by doping a pure silicon crystal with trivalent impurities like boron (B) (figure I-4), gallium (Ga), and iridium (Id). The newly generated lattice's covalent bonds cannot be completed by the current number of electrons. A hole (+) is the term for the resulting void. A free electron is accepted by the vacancy. So, the term "acceptor atoms" refers to the trivalent dispersed impurities [3].

I-2-4-2 N-TYPE MATERIAL:

When pentavalent impurities are added to silicon or Ge, such as phosphorous (P), arsenic (As), or antimony (Sb) (figure I-4). While the fifth valence electron is just loosely attached to the nucleus, the other four valence electrons make four covalent bonds with the other four nearby Si or Ge atoms. The fifth electron needs very little energy to separate from its nucleus and become free to conduct. Hence, donor impurities are another name for pentavalent impurities. The band gap just below the conduction band contains the energy level corresponding to the fifth valence electron [4].

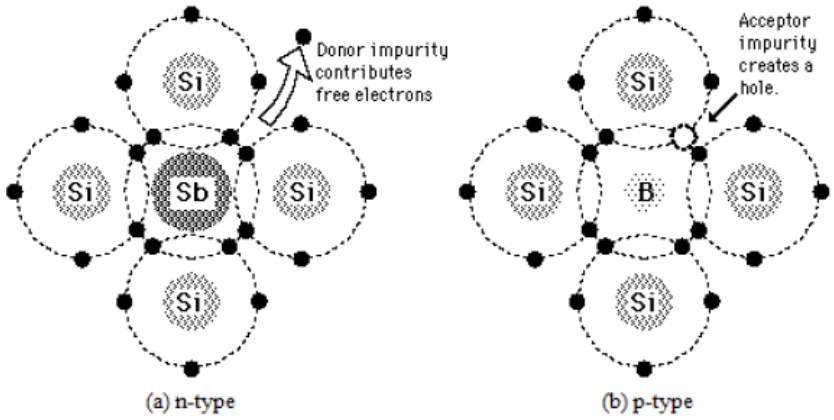

Figure (I-4): Extrinsic semi-conductor (a) n-type (b) p-type [4].

I-2-5 FERMI LEVEL:

The energy state or level known as the Fermi level is one that has a 50% chance of being occupied by an electron. The Fermi level for an intrinsic semi-conductor is located in the middle of the valence band and conduction band. All energy states above the Fermi level are empty at absolute zero, while all energy states below the Fermi level are full or occupied. Certain covalent bonds break at higher temperatures, releasing electrons that move into the conduction band. Because of this, when the temperature rises, the Fermi level shifts upward [2].

Donor impurities make an increase in the number of electrons in the conduction band of N-type semi-conductors. As a result, the Fermi level rises and approaches the conduction band (figure I-5).

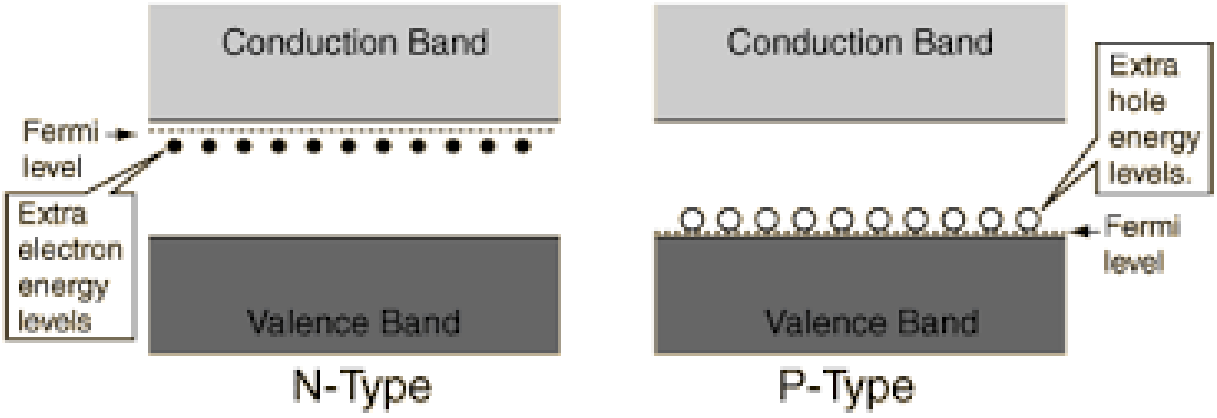

Figure (I-5): Fermi level in n-type and p-type semi-conductors [3].

The Fermi level E_F for N-type material can be written as:

$$E_F = E_C \times KT \ln\left(\frac{N_C}{N_D}\right) \quad \textbf{(I-1)}$$

E_F : Fermi level.

E_c : Energy level of conduction band.

K : Boltzmann's constant.

T : Temperature K.

N_C : Number of electrons in conduction band.

N_D : Concentration of donor impurity.

Because of acceptor impurities, a P-type semi-conductor's conduction band has fewer electrons than it does. As a result, the Fermi level decreases and approaches the valence band (figure I-5). The Fermi level of a P-type material can be written as:

$$E_F = E_V \times KT \ln(\frac{N_V}{N_A}) \quad \textbf{(I-2)}$$

E_F : Fermi level

E_V : Energy level of valence band

K : Boltzmann's constant

T : Temperature K

N_V : Number of electrons in valence band

N_A : Concentration of acceptor impurity

I-2-6 PN JUNCTION:

P-type semi-conductors have a majority of charge carriers in the form of holes since there are more holes in the valance band than there are electrons in the conduction band. Similarly, the N-type semi-conductor has a higher number of electrons in the conduction band than it has of holes in the valance band, which results in the majority of the charge being carried by electrons. Therefore, in its crystal structure, a P-type semi-conductor is made up of neutral immobile Si atoms, negative charged immobile impurity ions (acceptor ions), and positive charged holes acting as the majority charge carriers. Similar to this, the crystal structure of an N-type semi-conductor is made up of neutral immobile Si atoms, positively charged impurity ions (donor ions), and negatively charged electrons acting as the bulk of the charge carriers. In addition, P-type semi-conductors have little amounts of free electrons and N-type semi-conductors have a little amount of holes as minority charge carriers because of the ambient temperature [6].

When we put a semi-conductor of N type in contact with another one of P type (figure I-6), due to the concentration differential between the p- and n- sides, holes diffuse from the p-side to the n-side (p→n) and electrons diffuse from the n-side to the p-side (n→p) during the creation of a p-n junction. This charge movement causes diffusion current to flow across the junction. When an electron diffuses from n→p, it leaves an ionised donor on the n-side behind. Because it is bound to the surrounding atoms, this ionised donor (positive charge) is immobile. As electrons continue to flow from n→p, a layer of positive charge develops on the n-side of the junction. Similarly, when a hole diffuses from p→n as a result of the concentration gradient, it leaves behind an immobile ionised acceptor (negative charge). As the holes continue to disperse, a layer of negative charge develops on the p-side of the junction. Because the electrons and holes involved in the initial movement across the junction depleted the region of their free charges, this space-charge zone on each side of the junction is known as the depletion region. An electric field oriented from positive charge to negative charge emerges as a result of the positive space-charge area on the n-side of the junction and the negative space-charge region on the p-side of the junction. This field causes an electron on the p-side of the junction to travel to the n-side and a hole on the n-side of the junction to go to the p side. Drift is the mobility of

charge carriers caused by an electric field. As a result, a drift current, which is the opposite in direction to the diffusion current, begins [7].

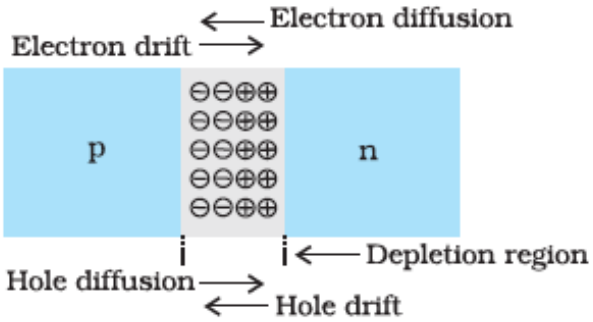

Figure (I-6): p-n Junction formation process [7].

I-2-6-1 BUILDING A P-N JUNCTION DIODE:

A P-N junction is made by attaching a P-type semi-conductor piece to an N-type semi-conductor piece so that the crystal structure stays continuous at the border. A semi-conductor diode (figure I-7) is a device with a single P-N junction [6].

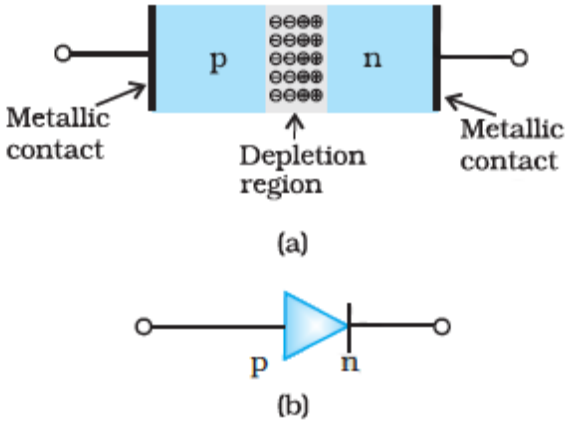

Figure (I-7): (a) Semi-conductor diode (b) Symbol for p-n junction [7].

Even in the absence of any external voltage source connecting the junction, this depletion zone creates a potential difference across the junction (abbreviated as VB). We refer to this electric potential (VB) as barrier potential or junction potential (figure I-8). For Si and Ge diodes, the junction potential or barrier voltage is 0.7 V and 0.3 V, respectively, at room temperature [6].

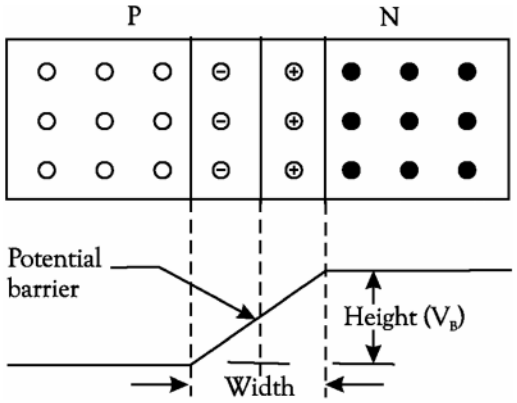

Figure (I-8): junction potential or barrier voltage of a p-n junction diode [6].

I-2-6-2 UNBIASED (NON-POLARIZED) P-N JUNCTION:

Diffusion of majority charge carriers occurs when P- and N-type semi-conductors are in electric contact, moving from the region of high to the region of lower concentration. This indicates that although holes migrate from the P to the N side of the junction as majority charge carriers in P-type semi-conductors, electrons, as the majority charge carriers in N-type semi-conductors, move from the N side to the P side. In the process of diffusion, holes come into contact with a lot of free electrons, collide, and recombine. In the same way, as free electrons diffuse from N-type to P-type semi-conductors, they crash and recombine with the holes.

As a result of the recombination, a depletion zone containing the PN junction forms, devoid of free charge carriers (figure I-9).

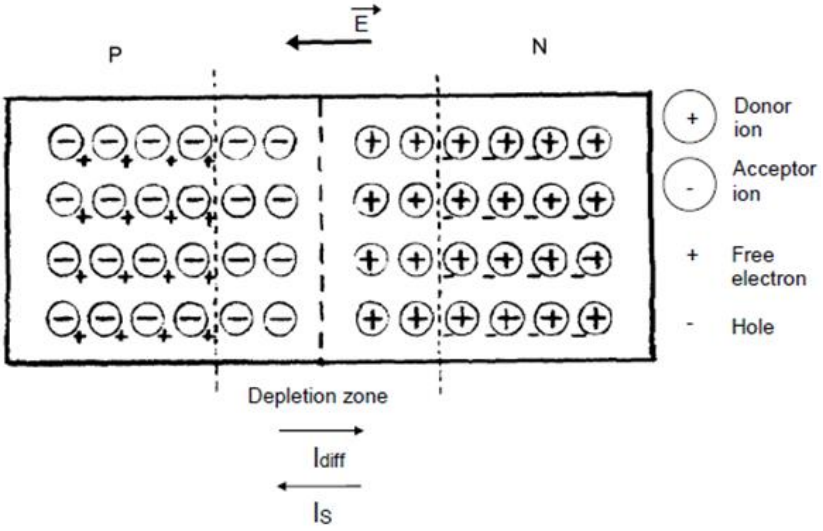

Figure (I-9): Unbiased (non-polarized) p-n junction [8].

As a result, the P side of the junction has positive fixed charge (donor ions) and the N side has negative fixed charge (acceptor ions). Because they are locked within the crystal lattice, these ions are immobile. As a result, there is an opposite electric charge on both sides of the PN junction, which creates an electric field and a potential barrier. The depletion zone, also known as the PN barrier, is the region where acceptor and donor ions are the only sources of fixed charge and there are no free charge carriers.

Thus, an electric field is created over the unbiased (non-polarized) PN junction's depletion zone. In the absence of an external voltage, a PN junction is unbiased. The majority of charge carriers' diffusion is resisted by this electric field. In addition to the majority charge carriers, semiconductors also contain minority charge carriers, which are holes in N semiconductors and electrons in P semiconductors. Minority charge carriers are accelerated across the depletion zone by the electric field across the PN junction, creating drift currents of minority charge carriers. Diffusion current, on the other hand, runs in the opposite direction of drift current and is produced by majority charge carriers. Diffusion between the P and N sides of the PN junction changes the majority free charge concentration and, consequently, the Fermi level in all semiconductor types. Free charge moves forward until both semiconductor types attain equilibrium and their Fermi levels equalise. There is no net current through the PN junction when the diffusion and drift currents are in equilibrium because they are the same and flowing in opposing directions [8].

I-2-6-3 BIASED (POLARISED) PN JUNCTION:

A biased P-N junction is one that is coupled to an outside voltage source. In electronics, a P-N junction like this has several uses. The width of the depletion region and, consequently, the current passing through the P-N junction can be regulated by applying an external voltage.

The external voltage source can be connected across the P-N junction diode in two different ways. They are as follows:

I-2-6-3-1 FORWARD BIAS:

The positive terminal of the external voltage source (battery) is linked to the P-type region of the diode, while the negative terminal is connected to the N-type region of the diode (figure I-10). This arrangement narrows the depletion region (resulting in a lower V_B) and allows a considerable quantity of current to flow through the junction. In actuality, the external applied potential must be larger than the diode's barrier potential in order to forward bias a P-N junction and conduct current [6].

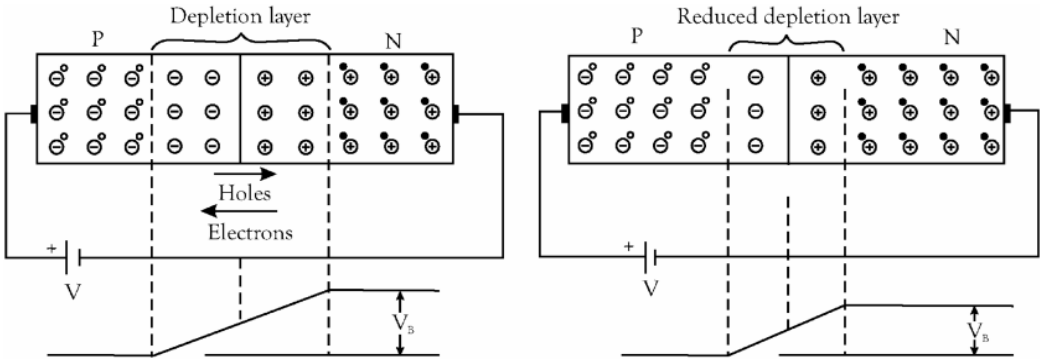

Figure (I-10): P-N junction with forward bias [6].

I-2-6-3-2 REVERSE BIAS:

When an external voltage source (battery) is used in reverse bias, its positive terminal is connected to the N-type region of the diode and its negative terminal is connected to the P-type region (figure I-11). With this arrangement, the depletion region is wider and the junction is not conducting current (which leads to an increase in V_B). However, because minority charge carriers are available, a tiny amount of current passes through the reverse biassed junction at room temperature. Reverse saturation current is what it is known as, and it rises as temperature does [6].

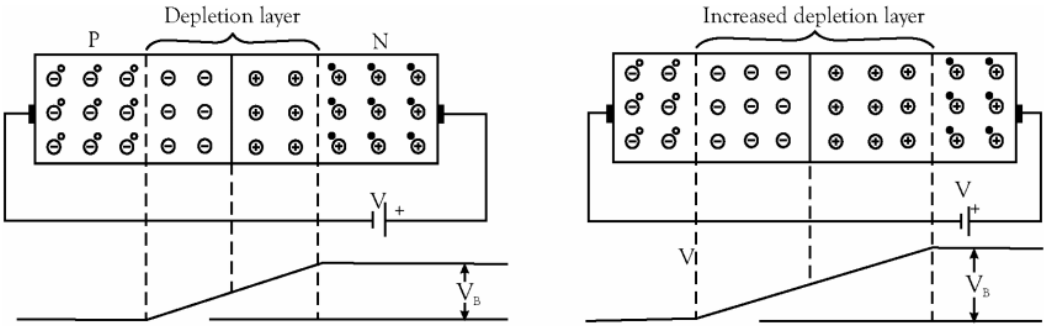

Figure (I-11): P-N junction with reverse bias [6].

I-2-6-4 CHARACTERISTICS OF SEMI CONDUCTOR DIODE:

I-2-6-4-1 FORWARD:

Not much current flows through the diode at first when it is forward-biased and the applied voltage is increased from zero (Figure I-12). This is because the internal barrier voltage (VB), which has a value of 0.3 V for Ge and 0.7 V for Si, opposes the external voltage. Current via the diode quickly rises with applied battery voltage as soon as VB is neutralised. It is

discovered that a forward current of roughly 50 mA is produced by a little voltage of 1.0 V. Over a safe limit, the forward voltage will cause the diode to burn and stop working. Knee voltage is the forward voltage at which the current IB begins to flow [6].

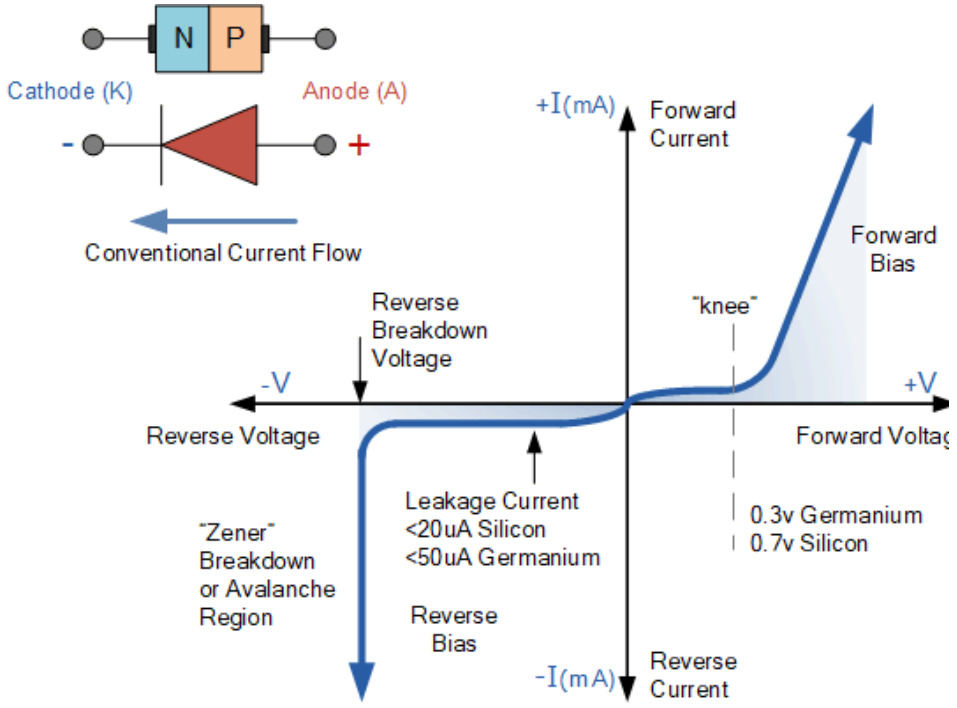

Figure (I-12): Junction diode symbol and static I-V (current-voltage) characteristics.

I-2-6-4-2 REVERSE:

Reverse-biasing the diode results in the blocking of majority carriers and minimal current flow through the diode (caused by minority charge carriers). The reverse current, sometimes referred to as leakage current, rapidly approaches its maximum or saturation value when the reverse voltage rises from zero (figure I-12). For Si, it is on the order of nanoamperes, and for Ge, it is microamperes. The leakage current increases suddenly as the reverse voltage rises above a certain value known as the breakdown voltage V_{BR}. At this point, the curve represents zero resistance [6].

I-2-6-5 THE DIODE EQUATION:

The current flowing through a p-n junction under forward and reverse bias is provided by the diode equation [5].

$$I = I_0\left(\frac{qV}{e^{\eta KT}} - 1\right) \qquad \textbf{(I-3)}$$

I : The net current flowing through the diode.

I_0 : The diode leakage current density in the absence of light.

V : Applied voltage across the terminals of the diode.

q : Absolute value of electron charge.

K : Boltzmann's constant.

T : Absolute temperature (K).

η : Ideality factor (a number between 1 and 2 which typically increases as the current decreases. At low current, $\eta = 1$ for germanium diode and $\eta = 2$ for silicon diode).

I-2-6-6- PN DIODE ENERGY BAND DIAGRAM:

It is evident that the energy levels of the valence and conduction bands in the n region are lower than those in the p region. It is simple for the free electrons in the n region, which have the highest energy density in the conduction band, to diffuse across the junction and momentarily transform into free electrons in the lower conduction band of the p-region (figure I-13-a-). The electrons swiftly lose energy after passing the connection and drop into the p-region valence band holes. The n-region conduction band's energy level falls as the diffusion process progresses and the depletion area starts to form. Higher-energy electrons that have diffused across the junction to the p region are lost, which results in a drop in the energy level of the conduction band in the n region. The alignment of the top of the n-region conduction band and the bottom of the p-region conduction band indicates that soon there are no more electrons in the n-region conduction band with sufficient energy to bridge the junction to the p-region conduction band. Since diffusion has stopped, the junction is now at equilibrium, and the depletion region is full (figure I-13-b-) [9].

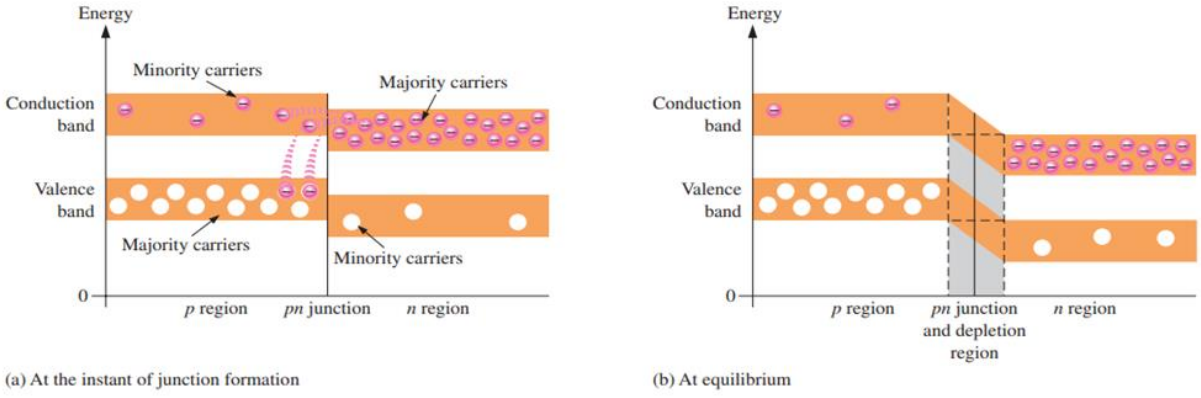

Figure (I-13): Energy diagrams illustrating the formation of the P-N junction and depletion Region (a) at the instant of junction formation (b) at equilibrium [9].

I-2-7 APPLICATIONS OF SEMI-CONDUCTORS IN SOLAR CELLS:

The absorption of photons as a result of the formation of charge carriers and the subsequent separation of the photo-generated charge carriers occur in semi-conductor materials in the majority of solar cells nowadays. As a result, the semi-conductor layers, which comprise the bulk of the solar cell, are its most crucial components. The conversion of photon energy into electrical energy can be accomplished with a variety of semi-conductor materials.

The following are the key semi-conductor factors that influence the design and performance of a solar cell:

i) Concentrations of doping atoms, which can be of two different types; donor atoms which donate free electrons, N_D, or acceptor atoms, which accept electrons, N_A. The concentrations determine the width of a space-charge region of a junction.

ii) Mobility, μ, and diffusion coefficient, D, of charge carriers that characterize carriers transport due to drift and diffusion, respectively.

iii) Lifetime, τ, and diffusion length, L, of the excess carriers that characterize the recombination-generation processes.

iv) Band gap energy, Eg, absorption coefficient, α, and refractive index, n, that characterize the ability of a semiconductor to absorb visible and other radiation [10].

I-3 SOLAR RADIATION:

I-3-1 ENERGY RESOURCES:

Energy is broadly classifying into two main groups: Renewable and Non-renewable.

I-3-1-1 NON-RENEWABLE ENERGY:

Energy derived from fossil fuels, including coal, crude oil, natural gas, and uranium, is classified as non-renewable energy. Non-renewable energy requires human intervention to make it fit for use, in contrast to renewable energy. Fossil fuels are essentially made up of carbon. Fossil fuels are thought to have developed more than 300 million years ago, when the earth's surface was very different [11].

I-3-1-1-1 NON-RENEWABLE ENERGY TYPES:

Fuels derived from fossil deposits make up the majority of non-renewable energy resources. The non-renewable resources that are most prevalent include:

- Petroleum products
- Coal.
- Compressed natural gas.

Apart from fossil fuels, nuclear fuels are also non-renewable [11].

I-3-1-2 RENEWABLE ENERGY:

Renewable energy is derived from natural sources such as plants, the sun, wind, water, and the heat from the Earth. Through the use of renewable energy technology, these fuels can be converted into useful energy sources, such as electricity, heat, chemicals, or mechanical power [12].

I-3-1-2-1 RENEWABLE ENERGY TYPES:

Renewable energy sources are not depleted and are distributed across a large geographical area; these resources are rapidly regenerated through natural processes. It will not cause any environmental pollution. The fundamental advantage of adopting renewable resources is that they are available all year. We can draw energy for many decades without hurting the environment by making a one-time investment [13].

The renewable resources that are most prevalent include:

- Solar energy.
- Wind energy.
- Biomass energy.
- Tidal power.
- Geothermal energy.

I-3-2 THE SUN:

The sun is the nearest star to Earth, and its radiant light is the only source of energy that controls atmospheric motions and our climate. The sun is a totally gaseous mass primarily made of hydrogen. It has a complicated physical structure that may be divided into various regions: the core, the interior, the convection zone, the photosphere, the reverse layer, the chromosphere, and the corona (figure I-14) [14].

The Sun's surface temperature ranges from 5600 to 6000 K [15].

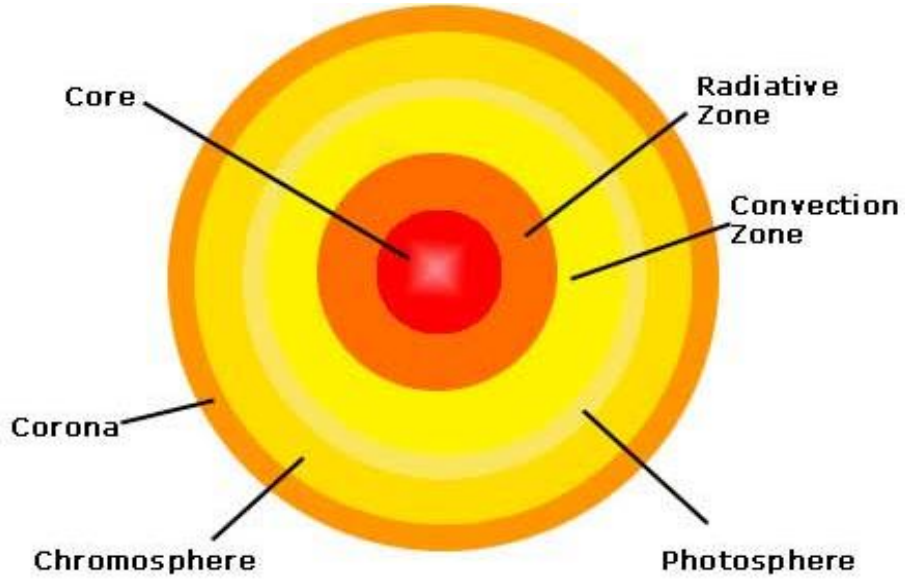

Figure (I-14): Anatomy of the sun.

I-3-3 SUN-EARTH DISTANCE:

The earth revolves in an oval orbit around the sun (figure I-15). The amount of solar energy that reaches the planet is inversely related to its squared distance from the sun; thus, a correct sun-earth distance is required. The mean sun-earth distance r_0 is known as one astronomical unit (1 AU = 1.496 x 10^8 Km).

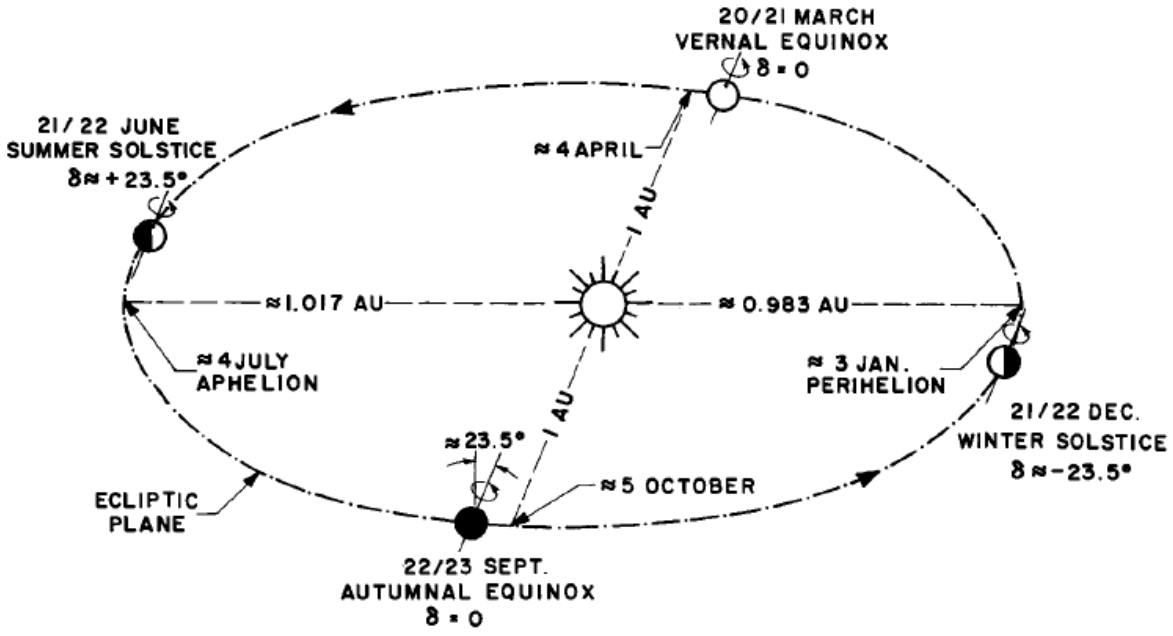

Figure (I-15): Motion of the earth around the sun [14].

The smallest sun-earth distance is 0.983 AU , while the maximum is 1.017 AU .The earth reaches its closest point to the sun (perihelion) on roughly 3th January and its furthest point (aphelion) on approximately 4th July. The earth's average distance from the sun occurs between 4th April and 5th October [14].

High accuracy has been achieved in determining the light time for the astronomical unit of distance τ , which is the average time it takes for light to travel between the Sun and Earth. It's important to commit the approximate value which is accurate to within 0.2% to memory for all practical uses of solar energy(τ =500s) [15].

I-3-4 SOLAR CONSTANT:

The amount of incoming solar radiation, or insolation, at the top of the Earth's atmosphere has been measured by satellite during a 22-year period, and the result is 1366 $J/(m^2 \times s)$ [16].

I-3-5 SOLAR DECLINATION:

An angle of up to ± 23,45° will separate the solar altitude angle recorded at midday from the appropriate equinoctial angle. We refer to this angle as the solar declination (figure I-16). Its definition is the angular separation between the sun at solar noon and the observer's zenith at the equator. When it points north, it is positive; when it points south, it is negative. On 21st June, which is the summer solstice in the northern hemisphere and the winter solstice in the southern hemisphere, the declination reaches its greatest value of +23.45°, 20th December is the day that the minimum value -23.45 is reached.

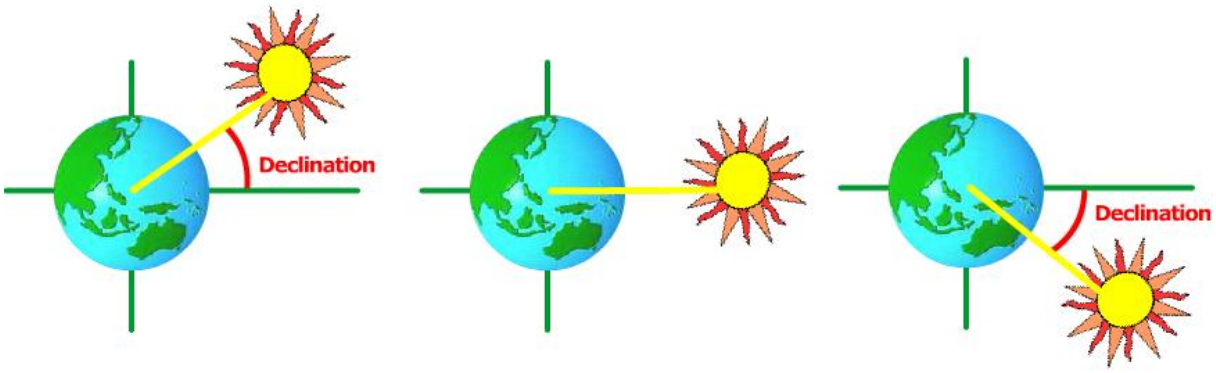

Figure (I-16): Declination angle.

The following formula can be used to determine the declination, expressed in degrees, on any given day in first approximation: [17]

$$\delta = 23,45° \times \sin\left[\left(\frac{360}{365}\right) \times (d + 284)\right] \quad \textbf{(I-4)}$$

where d is the day of the year with Jan 1 as $d = 1$

I-3-6 ROTATION OF EARTH:

The visible position of the Sun in the sky varies over time due to Earth's rotation and orbital motion around the Sun. In order to make the most use of solar energy, we need to comprehend how the Sun appears to move.

Earth can be viewed as a perfect sphere rotating on a fixed axis at a constant angular velocity for the sake of solar energy applications. The North and South Poles are the two locations on Earth's surface where the axis of rotation passes through. The equator is the vast circle that is perpendicular to the axis. The latitude φ and longitude λ, which are indicated on (figure I-17) and may be found via GPS (the Global Positioning System), can be used to specify a place on Earth [15].

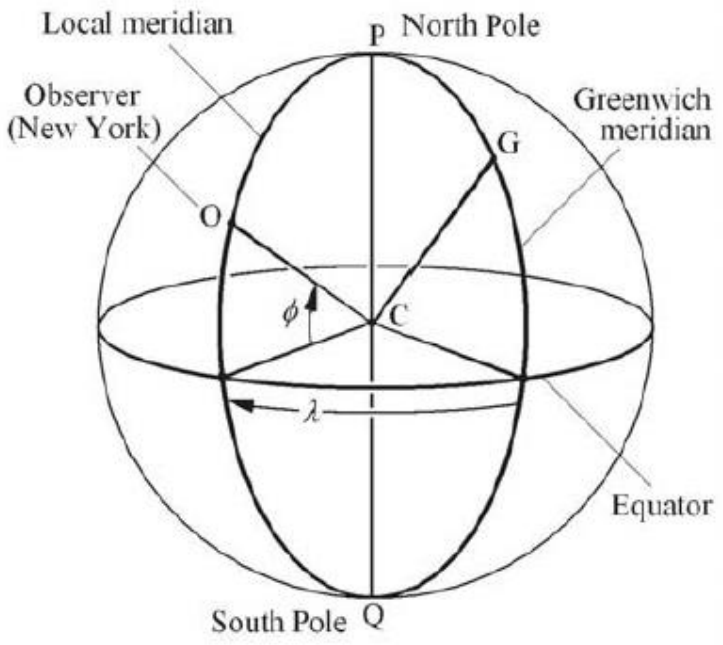

Figure (I-17): Rotation of Earth: Latitude and Longitude [15].

I-3-7 Relationship between the Atmosphere and Sunlight:

Thirty percent or so of solar light is dispersed or reflected back into space. Six percent is scattered by air, twenty percent is reflected by clouds, four percent is reflected by Earth's surface, and twenty percent is absorbed by the atmosphere, of which 16% absorbed by dust,

water vapour, and O_3. The cloud absorbs an additional 4%. The atmosphere warms as a result of the sun's energy absorption. The Earth's solid surface absorbs half of it (figure I-18).

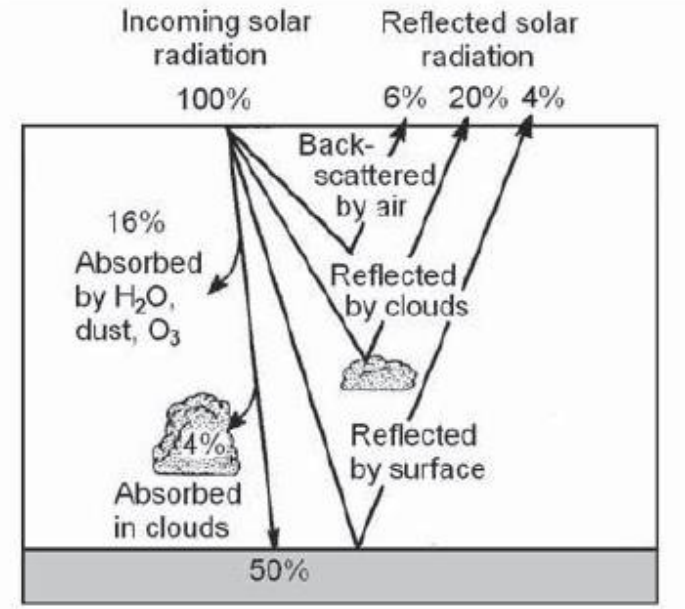

Figure (I-18): Interaction of sunlight with atmosphere [15].

The total radiation energy received by the atmosphere and the solid Earth is about 70%. Earth and its environs should be in thermal equilibrium. It is true that 70% of solar radiation that reaches Earth's atmosphere is reflected back into space as thermal radiation [15].

I-3-8 ATMOSPHERIC ATTENUATION:

Two processes can cause solar radiation with normal incidence to be attenuated as it travels through the atmosphere: scattering and absorption. When radiation interacts with the dust, water, and molecules of air in the atmosphere, scattering takes place. The wavelength of the radiation in relation to particle size, the concentration of particles in the atmosphere, and the total mass of air that the radiation must pass through all influence the degree of scattering. Rayleigh scattering, the process by which light is scattered off air molecules, is the most significant one. Shorter wavelengths in the blue end of the spectrum primarily those shorter than 0.6 μm are best suited for this kind of scattering. The blue sky during the day, the golden Sun, and the reddening of the sky at night are all explained by this scattering mechanism. This happens as a result of Rayleigh scattering, which disperses the majority of radiation that reaches the earth from sources other than the Sun. Observe that a considerable portion of the dispersed light is reflected back into space (figure I-19) [18].

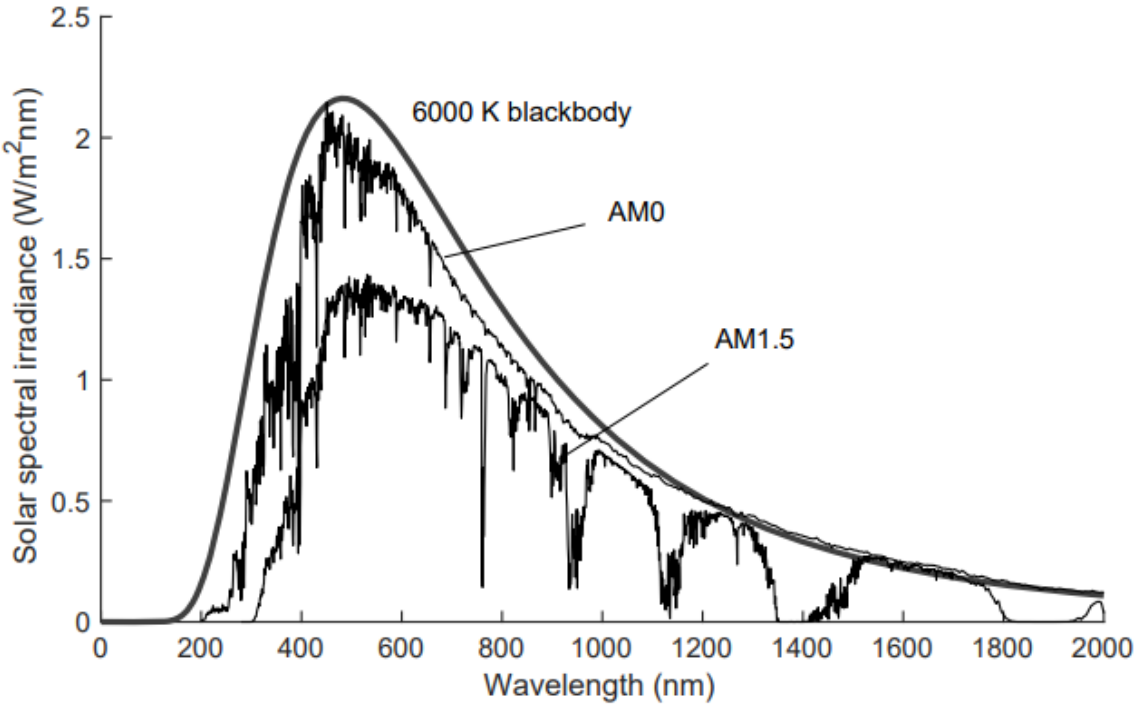

Figure (I-19): Spectral distribution of black body radiation and sun radiation [18].

I-3-9 AIR MASS:

The amount of time solar radiation must pass through the atmosphere before it is attenuated. The number of particles the light must contact with increases with journey length. This varies daily and throughout the year, with the longest path occurring in the evenings when the Sun is getting closer to the horizon. The air mass describes the journey length. In technical terms, air mass is the ratio of the mass of the atmosphere that the sun goes through to get from its current location in the sky to the mass it would pass through if it were at the zenith (directly overhead.)

The air mass is approximated to close to the angle θ_Z, which represents the angle from overhead to the Sun.

$$m = \frac{1}{\cos\theta_z} \qquad \textbf{(I-5)}$$

For the purpose of developing and testing solar devices, a standard spectrum for radiation at ground level is required since air conditions change over time. The *AM* 1.5 spectrum distribution for m = 1.5, which corresponds to a zenith angle of 48.2°, is the recognised standard (figure I-20) [17].

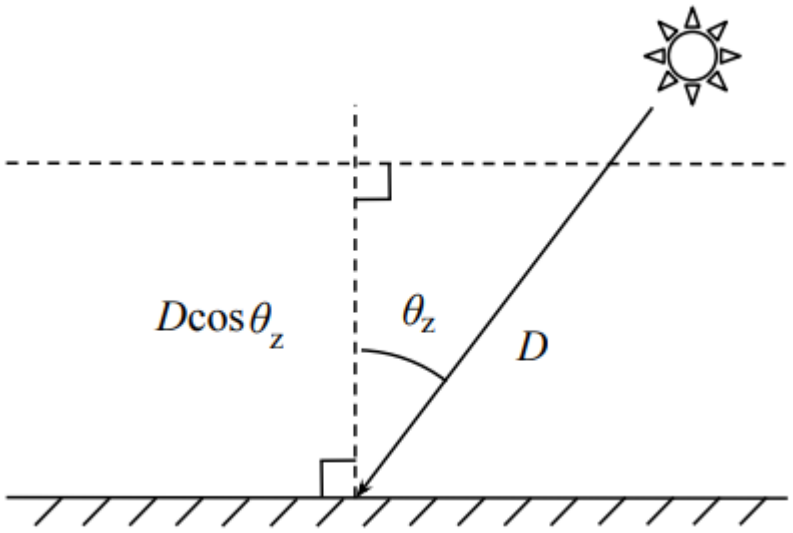

Figure (I-20): Atmospherical path length D of solar radiation at zenith angle [17].

I-3-10 IMPORTANCE OF SOLAR RADIATION MEASUREMENT:

Knowing the quantity of sunlight that is available at a given location at a given time is crucial for PV system design. Solar radiance and solar insolation are the two metrics most often used to characterise solar radiation. The instantaneous power density expressed in kilowatts per square metre is known as the sun radiance. Throughout the day, the solar radiance ranges from zero kW/m^2 at night to a maximum of over 1 kW/m^2. The location and weather have a significant impact on solar radiance.

I-3-11 MEASURING INCOMING SOLAR RADIATION:

Direct solar radiation from the sun and its marginal perimeter is measured with a pyrheliometer (figure I-21).

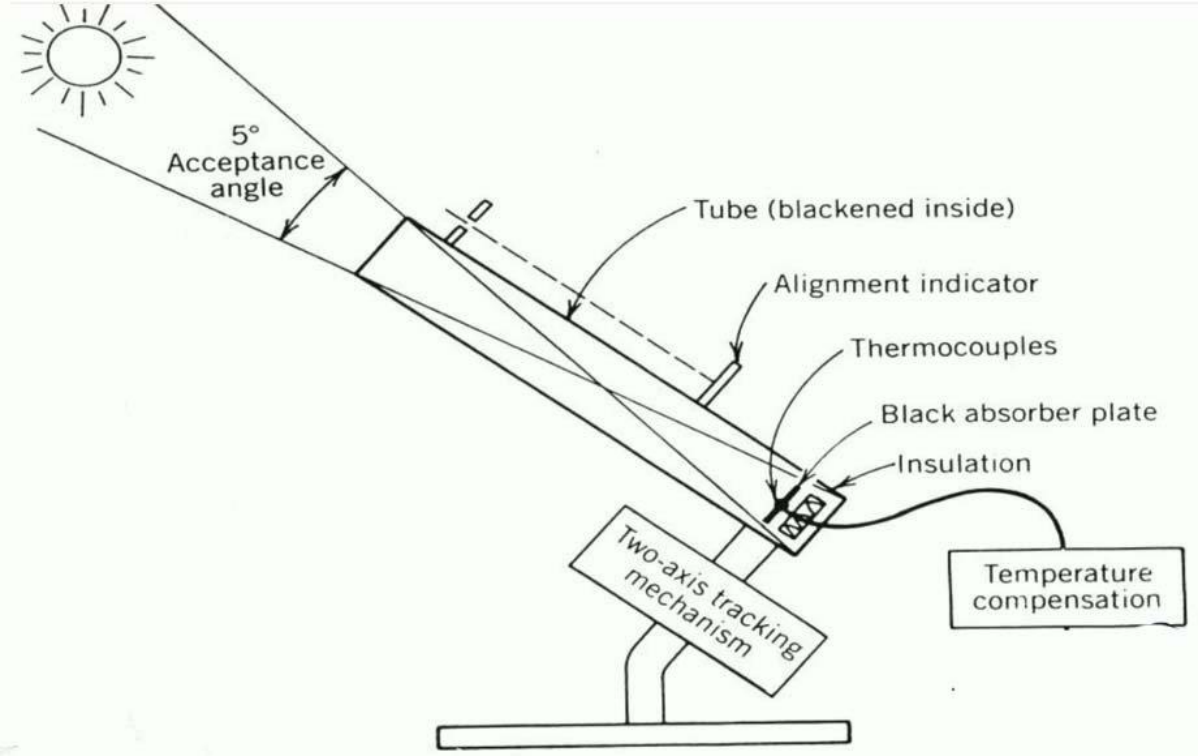

Figure (I-21): Pyrheliometer Construction [19].

Its receiving surface must be oriented so that it is normal to the direction of the sun in order to measure direct solar radiation accurately. Because of this, the instrument is typically mounted on an equatorial mount, which is a sun-tracking device. This is a trustworthy tool that has been used for a long time as a working standard to measure direct sun radiation, but using it manually calls for experience. This pyrheliometer features multiple diaphragms to allow only direct sunlight to reach the sensor, two manganin-strip sensors (20.0 mm × 2.0 mm × 0.02 mm), and a rectangular aperture. The sensor surface has uniform absorption properties for short-wave radiation and is painted optical black. Every sensor strip has a copper-constant thermocouple affixed to its back, which is linked to a galvanometer. When a current passes through the sensor strips, they also function as electric resistors and produce heat.

This kind of pyrheliometer only measures solar irradiance when one sensor strip is shielded from sunlight by a small shutter on the front face of the cylinder, allowing sunlight to reach the other sensor. Because one sensor strip absorbs solar light and the other does not, there is a temperature differential between the two. A thermoelectromotive force equivalent to this difference causes current flow through the galvanometer. After that, the colder sensor strip receives current until the galvanometer's pointer reads zero, at which point Joule heat balances the temperature increase caused by solar radiation. Now, the adjusted current is converted to

get a value for direct solar irradiation. If S is the intensity of direct solar irradiance and I is the current, then:

$$S = KI^2 \qquad \textbf{(I-6)}$$

where K is a constant intrinsic to the instrument and is determined from the size and electric resistance of the sensor strips and the absorption coefficient of their surfaces [19].

I-3-12 SPECTRAL CHARACTERISTICS OF SOLAR RADIATION:

Solar radiation is a radiant energy emitted by the Sun as a result of its nuclear fusion reactions. Spectral characteristics of solar radiation, both external to the Earth's atmosphere and at the ground, can be seen in (figure I-22). Over 99% of the energy flux from the Sun is in the spectral region of 0.15–4 μm, with approximately 50% in the visible light region of 0.4–0.7 μm. The total amount of energy emitted by the Sun and received at the extremity of the Earth's atmosphere is constant, that is, 1370 W/m^2/s. The amount of energy received per unit area of the Earth's surface is 343 W/m^2/s. The standard spectrum for space applications is referred to as AM_0. It has an integrated power of 1366.1 W/m2. Two standards are defined for terrestrial use: (1) the $AM_{1.5}$ global spectrum is designed for flat plate modules and has an integrated power of 1000 W/m2 and (2) the AM1.5 direct spectrum is defined for solar concentrator work [19].

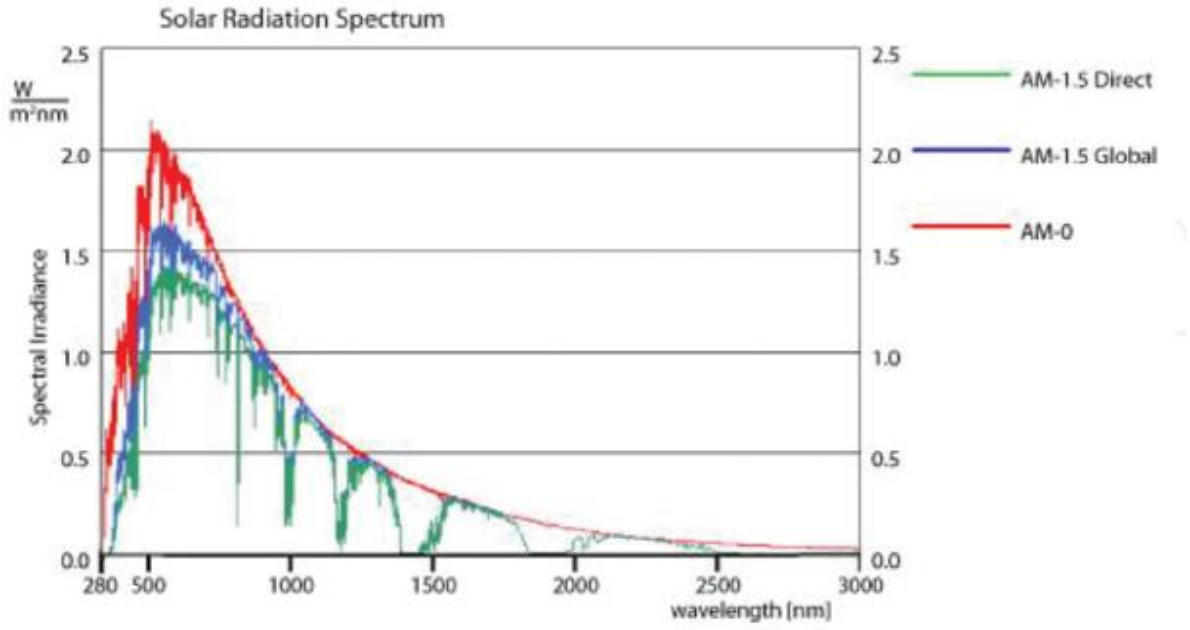

Figure (I-22): Spectral distribution of radiation intensity [20].

I-3-13 PHOTOVOLTAICS:

The technology known as photovoltaics uses photons to illuminate semiconductors to produce direct current (DC) electrical power, measured in Watts (W) or kilowatts (KW). The solar cell, which is the term for each individual PV element, produces electricity as long as light is shining on it. The electricity cuts off when the light goes out. Unlike batteries, solar cells never require recharging. Some have been operating outdoors continuously for more than 30 years, either on Earth or in space.

CHAPTER II: SOLAR CELLS

II-1 INTRODUCTION:

A solar cell, also known as a photovoltaic (PV) cell, is a device that uses the photovoltaic effect to directly convert light energy into electrical energy. It is an essential part of solar panels, which use sunlight to create power. Usually composed of semiconductor materials like silicon, solar cells function by absorbing photons, or light particles, from the sun. The photons then liberate electrons from atoms in the semiconductor material to produce an electric current.

II-2 SOLAR CELL STRUCTURE:

In the most of the solar cells, we can notice that the structure design is divide in different parts (figure II-1):

1. **Antireflective Layer (AR Layer):** The transparent layer at the top minimizes light reflection, allowing more sunlight to enter the cell.
2. **Metal Grid:** A thin grid of metal fingers collects current from the top surface of the cell. These fingers must be thin and spaced closely to allow sufficient sunlight to pass through and reach the absorber layer.
3. **N-Type Layer:** This layer is made from a semiconductor material doped with impurities to create an abundance of electrons (negative charge carriers).
4. **P-Type Layer:** This layer is made from the same semiconductor material doped with different impurities to create an abundance of holes (positive charge carriers).
5. **Metal Contact:** A layer of metal on the back surface that collects current from the n-type layer and forms the other electrical contact for the cell.

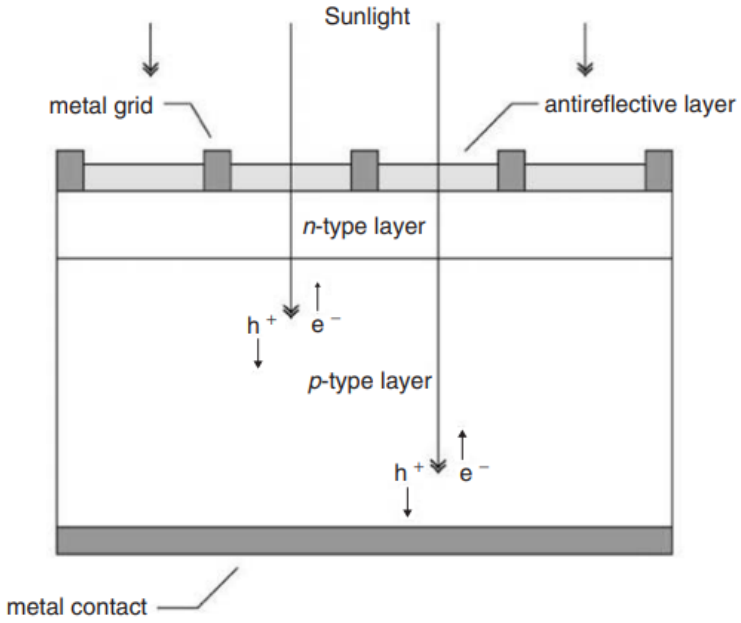

FIGURE (II-1): Solar cell structure [21].

II-3 FUNCTIONNING OF SOLAR CELL:

Photons of light can readily enter the p-n junction through the extremely thin p-type layer when light reaches the junction. The connection receives enough energy from the light energy in the form of photons to produce a large number of electron-hole pairs. The junction's state of thermal equilibrium is broken by the incident light. The n-type side of the junction can be rapidly reached by the free electrons in the depletion zone. similarly, the p-type side of the junction might rapidly experience holes in the depletion. The barrier potential of the junction prevents the newly formed free electrons from continuing to cross it once they reach the n-type side. Similar to this, once the freshly formed holes reach the p-type side, they are unable to cross the junction again since they have reached the same barrier potential. The p-n junction will function like a little battery cell as the concentration of holes increases on one side of the junction, the p-type side, and the concentration of electrons increases on the other, the n-type side. A voltage known as the photovoltaic voltage is set up. A minor current will flow across the junction if we attach a small load across it.

II-4 BASIC CHARACTERISTICS OF A SOLAR CELL:

At a certain photocurrent, an illuminated solar cell can produce a specific photovoltaic. A solar cell's working point is a set of photovoltaic and photocurrent values at which it can function. Because of Ohm's law, a solar cell's specific working point is fixed with a load resistance (R_L) [22].

$$R_L = \frac{U}{I} \qquad \textbf{(II-1)}$$

According to Ohm's law, at very low R_L, the photovoltage is very low and at very high R_L, the photocurrent is very low. A solar cell is said to be operating in both short- and open-circuit conditions when its resistance (R_L) is either indefinitely high or equal to zero. Short-circuit current (I_{SC}) and open-circuit voltage (V_{OC}) are the terms used to describe the photovoltaic and photocurrent values under short- and open-circuit situations, respectively. When a solar cell operates in both short- and open-circuit modes, its electric power is zero [22].

A solar cell's current-voltage characteristic, or I–V characteristic, is a plot of all potential operating points within a range that is taken into consideration. The schematic representation of a solar cell's I–V characteristic under illumination is shown in (figure II-2) [22].

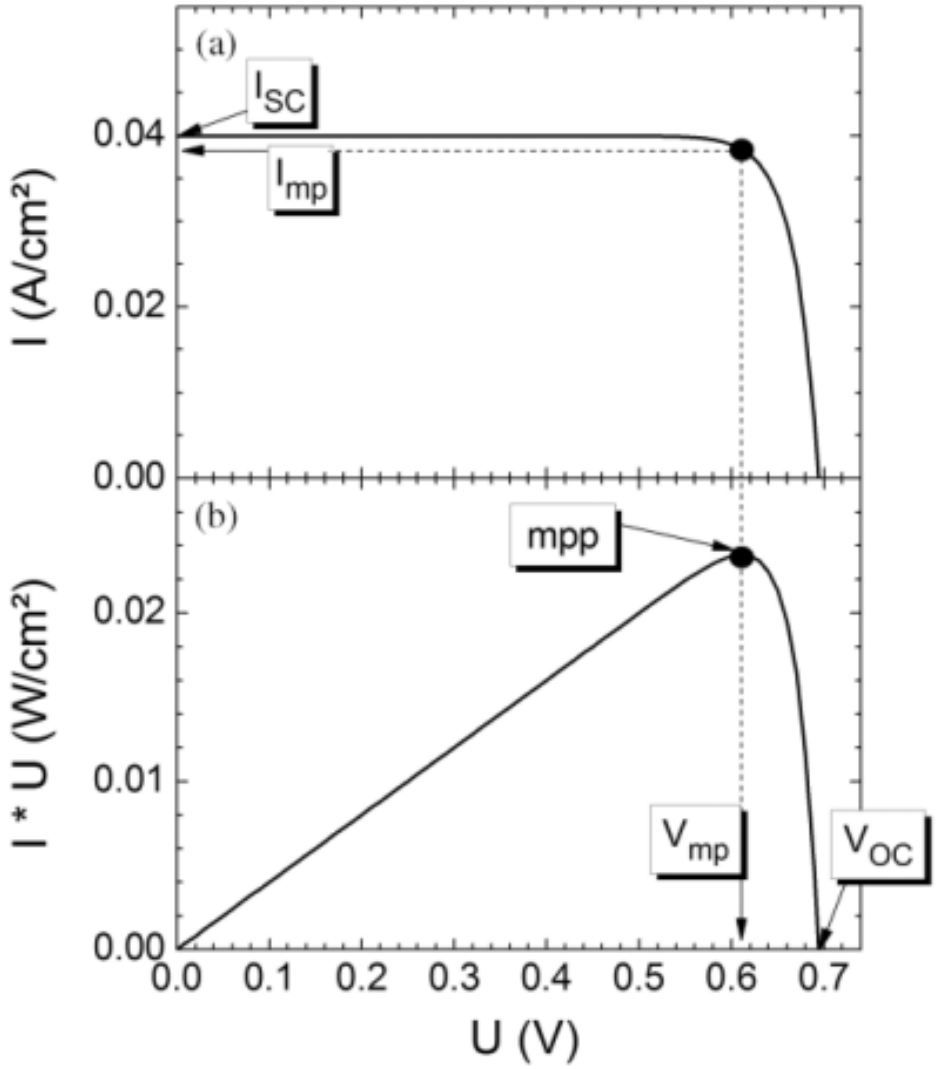

FIGURE (II-2): Example of a current–voltage characteristic (a) and of the corresponding power–voltage characteristic (b) of a solar cell under illumination (The short-circuit current density, the open-circuit voltage, the maximum power point and the voltage and current density at the maximum power point are denoted by I_{SC}, V_{OC}, mpp, V_{mp} and I_{mp}, respectively) [22].

The solar cell's maximum power can be achieved at a single voltage and current combination (V_{mp} and I_{mp}, respectively). This point on the I–V characteristic of an illuminated solar cell is called the maximum power point (mpp) [22].

$$P_{mpp} = I_{mp} \times U_{mp} \qquad \textbf{(II-2)}$$

Measuring the I_{SC} ,V_{OC} values is simple. Therefore, rather than characterising the solar cell with Imp and Ump, it is more convenient to characterise the maximum power of a solar cell with I_{SC}, V_{OC}, and an additional parameter. The additional parameter establishes the relationship between the product of I_{SC} and V_{OC} and the product of I_{mp} and U_{mp} .This parameter, also known as the fill factor (FF), indicates the degree to which the I_{mp} -U_{mp} rectangle fills the I_{SC} -V_{OC} rectangle [22].

$$FF = \frac{I_{mp} \times U_{mp}}{I_{sc} \times V_{oc}} \qquad \textbf{(II-3)}$$

The solar energy conversion (η) of solar cell is defined as the ratio between the power extracted at the mpp of the solar cell and the power of the sunlight at which the solar cell is illuminated (P_{SUN}) [22].

$$\eta = FF \frac{I_{SC} \times V_{OC}}{P_{SUN}} \qquad \textbf{(II-4)}$$

These characteristics are typically measured under standard test conditions (STC), which are a set of environmental conditions that are used to ensure consistent and comparable measurements of solar cell performance. Standard test conditions typically include an irradiance of 1000 W/m² and a cell temperature of 25°C [22].

II-5 EQUIVALENT CIRCUIT OF SOALR CELL:

II-5-1 IDEAL SOLAR CELL:

The equivalent circuit of the ideal solar cell consists of two distinct parts that represent the two basic functionalities of a solar cell. The photocurrent generator, or current source powered by light, is the first component. In order for the current to flow through the second element in one direction but not the other, it must satisfy the requirement of charge separation. This is the unique characteristic of a diode, the second component in the circuit equivalent to an ideal solar cell [21] (figure II-3).

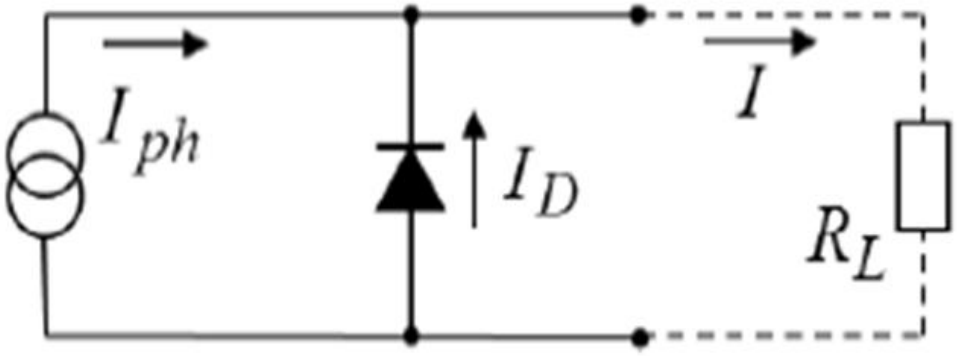

FIGURE (II-3): Equivalent circuit of an ideal solar cell containing a photocurrent generator and a diode for charge separation and connected to a R_L [22].

A current across a diode (I_D) is described by the diode equation:

$$I_D = I_0 \times \left[e^{\frac{q \times U}{K_B \times T}} - 1 \right] \qquad \textbf{(II-5)}$$

I_0: The diode saturation current.

K_B: Boltzmann's constant.

q: Charge of an electron.

U: the applied voltage.

T: Absolute temperature.

II-5-2 REAL SOLAR CELL:

Ohmic resistances cause losses in every solar cell. For example, in a solar cell, parallel resistances are caused by defects such as local shunts, while series resistances are caused by contact resistances or material resistances. The equivalent circuit of a real solar cell consists of one common series resistance (R_S) and one common parallel resistance (R_P), also known as shunt resistance (figure II-4).

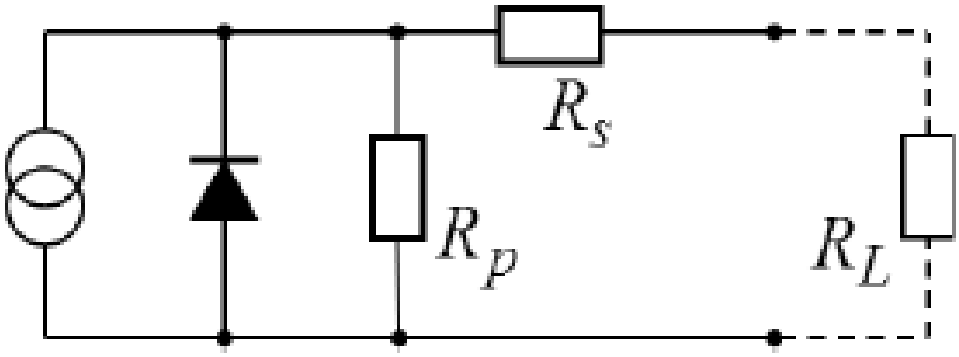

FIGURE (II-4): Equivalent circuit of a real solar cell containing a photocurrent generator, an ideal diode, a shunt resistance (R_P) and a series resistance (R_S) and being connected with a load resistance (R_L) [22].

There is an equal current passing through both the R_S and the R_L. Consequently, the voltage drops across the R_S reduces the potential across the R_L. Additionally, the current passing through the R_P lowers the current passing through the R_L. The diode equation below accounts for the voltage drop across R_S and the current shunted by R_P:

$$-I = I_0 \times \left[e^{\frac{q\times(U-I\times R_s)}{K_B\times T}} - 1 \right] + \frac{U - I \times R_s}{R_p} - I_{sc} \qquad \textbf{(II-6)}$$

II-6 GENERATIONS OF SOLAR CELLS:

II-6-1 FIRST GENERATION:

This term describes the traditional p-n junction solar system. This is usually constructed of silicon (both single- and polycrystalline), doped with other elements to give them a preferred electrical charge carrier preference (p or n). But in the past, different materials, like as germanium, were also used to make similar devices. With over 86% of the market for solar cells, first generation photovoltaic cells, sometimes referred to as silicon wafer-based solar cells, are the predominant technology used in the commercial production of solar cells. Their enormous efficiency makes them dominant. This is in spite of the high cost of production, which second generation cells aim to address [23].

II-6-1-1 SINGLE-CRYSTALLINE SILICON (C-SI):

The single crystals are frequently produced by the Czochralski method. Due to their cost and the fact that they are cut from cylindrical ingots, single-crystal wafer cells typically do not fill a square solar cell module entirely without generating a significant amount of wasted refined silicon. As a result, the majority of c-Si panels have gaps visible at each of the four cell corners. The efficiency of monocrystalline solar cells can reach 17% (figure II-5) [23].

II-6-1-2 POLYCRYSTALLINE SILICON (POLY-SI):

produced from enormous, properly cooled, molten silicon blocks known as "cast square ingots." Although they are less efficient, poly-silicon cells are less expensive to construct than single crystal silicon cells. Only about 10% efficiency may be achieved by polycrystalline semiconductors (figure II-5) [23].

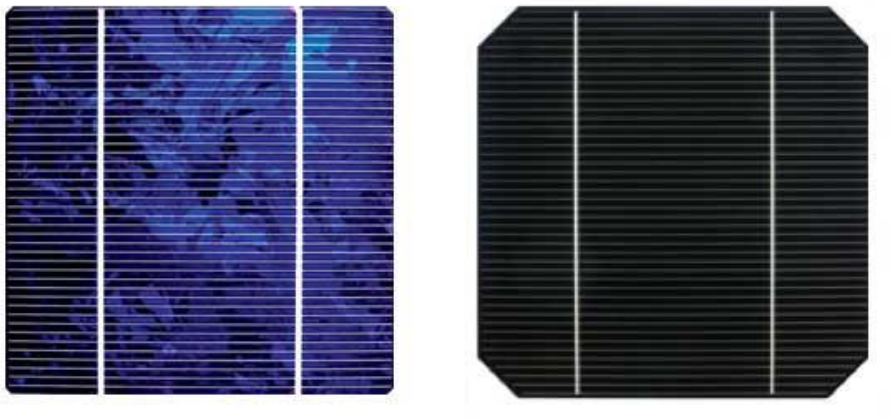

FIGURE (II-5): Single-crystalline and polycrystalline solar panels.

II-6-2 SECOND GENERATION (THIN FILMS SOLAR CELLS):

Thin films of photon-absorbers and layered stacks of thin films. It is capable of assembling several light-absorbing components into a "stack" of films, each of them may absorb a little different spectrum of light wavelengths than the films below it. Utilising a thin layer of material had the benefit of lowering the bulk of material needed for cell design. Thin-film solar cells often have lower efficiency than silicon (wafer-based) solar cells, but they also have lower production costs. Cadmium telluride (CdTe), copper indium gallium selenide, amorphous silicon, and micromorphous silicon have proven to be the most successful second-generation materials [23].

II-6-2-1 A CADMIUM TELLURIDE SOLAR CELL:

Uses a semiconductor layer called a thin film of Cadmium telluride (CdTe) to absorb light and turn it into electricity. If the cadmium in the cells were released, it would be toxic. Compared to CIGS and A-Si technologies, CdTe technology is roughly 30% and 40% less expensive, respectively.

II-6-2-2 COPPER INDIUM GALLIUM SELENIDE (CIGS):

Is a direct band gap material. Of all the thin-film materials, it has the highest efficiency (around 20%).

II-6-2-2-1 DIRECT BAND GAP:

In a material with a direct band gap, the lowest energy level in the conduction band and the highest energy level in the valence band have the same momentum. This allows light to directly excite an electron from the valence band to the conduction band, creating an electron-hole pair that can generate electricity (figure II-6).

II-6-2-2-2 INDIRECT BAND GAP:

In some materials, the momentum of the bands doesn't match. Here, an electron might need to absorb light and also interact with vibrations within the material to gain the necessary momentum and reach the conduction band. This indirect process is less efficient for generating electricity from light (figure II-6).

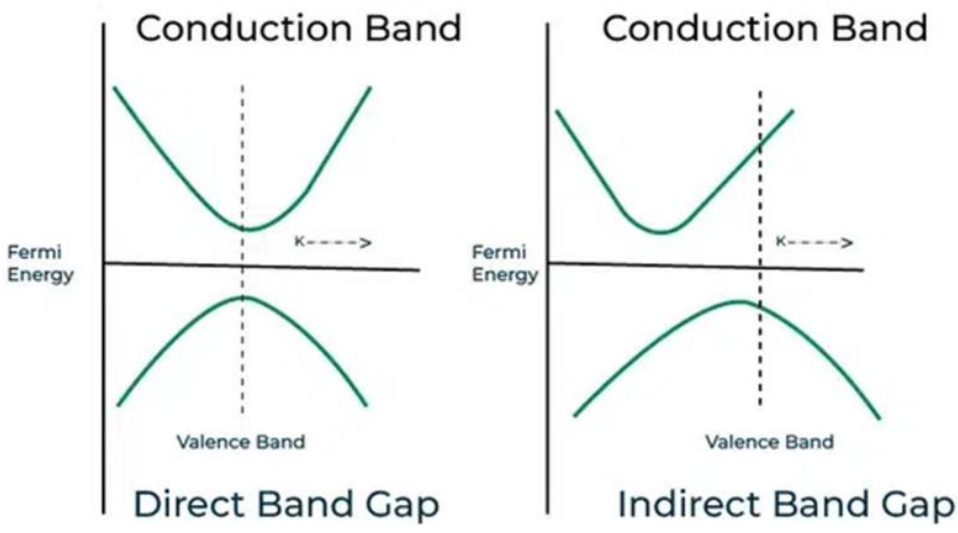

FIGURE (II-6): Direct and indirect band gap semiconductors.

II-6-2-3 AN AMORPHOUS SILICON (A-SI) SOLAR CELL :

Amorphous solar cells, often known as a-Si, are a widely used thin-film technology. Because they are made of thin layers rather than crystalline cells, their molecular structure is non-crystalline and their manufacture requires less energy (figure II-7).

FIGURE (II-7): Amorphous Silicon solar cell.

Because it requires less semiconductor material and produces fewer pollutants during production, this kind of cell is less expensive than the first generation. Because amorphous silicon cells are composed of extremely thin layers, they can absorb solar radiation up to 100 times better than crystalline ones.

II-6-3 THIRD GENERATION:

While keeping extremely low production costs, third generation technologies aim to improve the subpar electrical performance of second generation (thin-film technologies). Third generation cells typically consist of solar cells that do not require the p-n junction seen in silicon-based, conventional semiconductor cells. Polymer solar cells, nanocrystalline solar cells, and dye-sensitized solar cells are only a few of the many possible solar innovations found in third generation solar technology [23].

II-7 SERIES AND PARALLEL CONNECTIONS OF SOLAR CELLS:

Solar panels consist of multiple solar cells connected together electrically. The way these cells are connected determines the overall voltage and current output of the panel, which ultimately affects the power generation.

II-7-1 SERIES CONNECTIONS OF SOLAR CELLS:

We can first join them in a series connection. Voltages in a series connection build up. A string of three cells will result in an open circuit voltage of 1.8 V, for instance, if the open circuit voltage of one cell is equal to 0.6 V (figure II-8) [24].

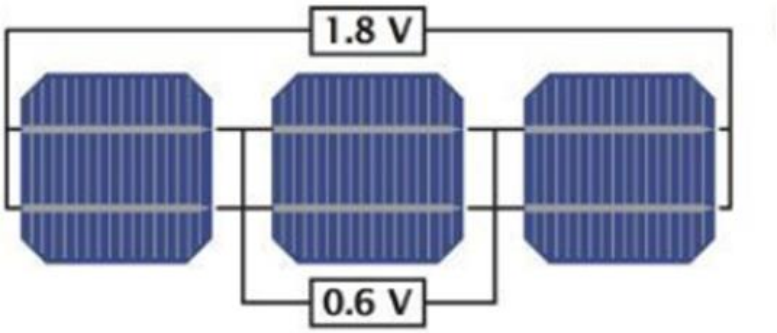

FIGURE (II-8): A series connection of three solar cells [24].

The I-V curve of solar cells connected in series is displayed in (figure II-9). When two solar cells are connected in series, the current remains constant but the voltages increase. The voltage across the open circuit that results is twice that of a single cell. Three solar cells connected in series result in an open circuit voltage three times higher than the current of a single sun cell [24].

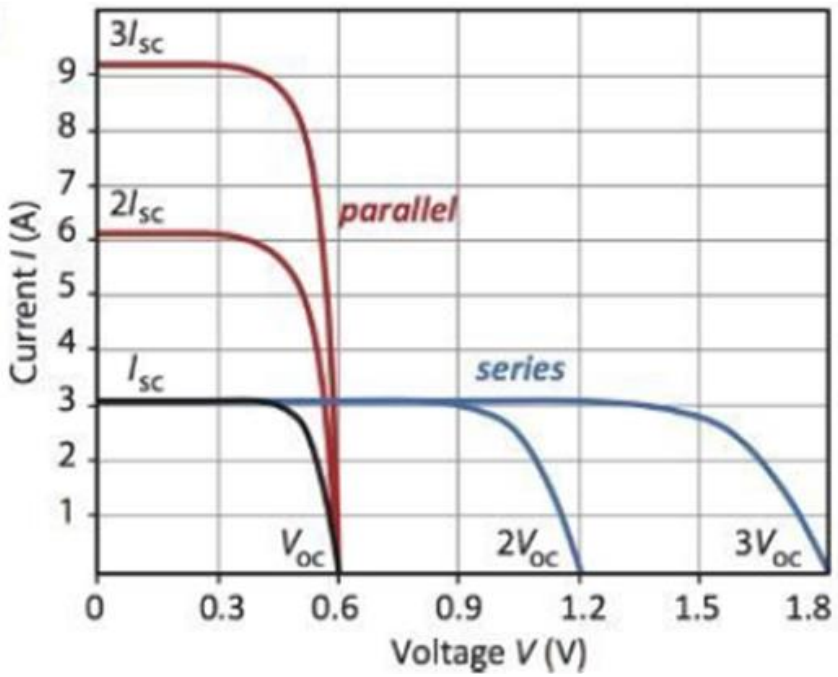

FIGURE (II-9): I-V curves of solar cells connected in series and parallel [24].

II-7-2 PARALLEL CONNECTIONS OF SOLAR CELLS:

We can connect solar cells in parallel, as shown in (figure II-10), which displays three solar cells connected in parallel. When solar cells are joined in parallel, their individual currents add up, but the voltage remains constant across the board.

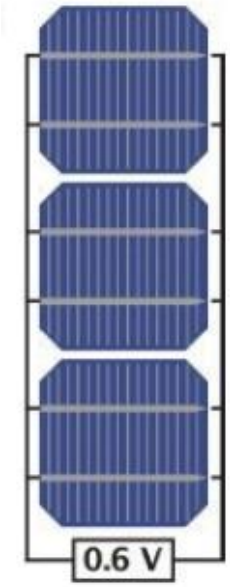

FIGURE (II-10): A parallel connection of three solar cells [24].

As shown in (figure II-9), for example, connecting three cells in parallel that have the same I-V characteristics results in three times the current and the same voltage as a single cell [24].

II-8 FACTORS AFFECTING CONVERSION EFFICIENCY

Not every photon of sunshine that enters a photovoltaic cell is turned into energy. Actually, the most of it is gone. A solar cell's capacity to convert the sunlight it receives is limited by a number of design variables. Increasing efficiency can be attained by designing with these considerations in mind.

II-8-1 WAVELENGTH:

The energy packets that make up light, known as photons, come in a variety of energies and wavelengths. The wavelengths of sunlight that reach the surface of the planet span from ultraviolet to infrared. Certain photons of light are reflected off a solar cell's surface, whereas other photons simply pass through. A portion of the photons that are absorbed convert to heat. The rest possess sufficient energy to liberate electrons from their atomic bonds, resulting in the production of charge carriers and electric current.

II-8-2 RECOMBINATION:

A "charge carrier," like a negatively charged electron, can move across a semiconductor material to allow electric current to flow through it. An additional example of a charge carrier is a "hole," which functions as a positive charge carrier and symbolises the lack of an electron in the substance. A hole can cause an electron to recombine, cancelling out the electron's contribution to the electrical current. The process via which electricity is produced in a solar cell is reversed by direct recombination, in which light-generated electrons and holes come into contact, recombine, and release a photon. It is among the basic elements that restricts effectiveness. When electrons or holes come into contact with an impurity, a crystal structural defect, or an interface that facilitates their recombination and subsequent release of energy as heat, this process is known as indirect recombination (figure II-11).

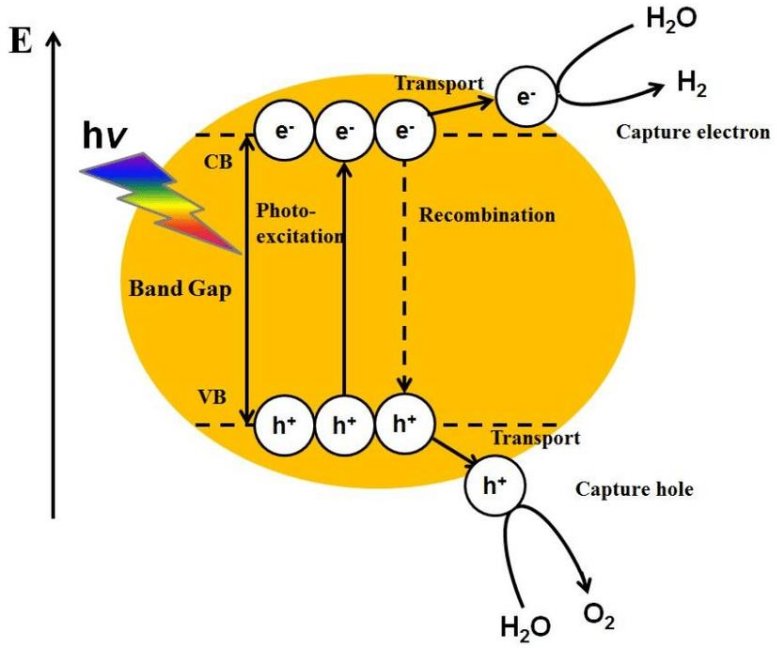

FIGURE (II-11): Mechanism of electron-hole pair formation, recombination and transport in a semiconductor.

II-8-3 TEMPERATURE:

Low temperatures are often ideal for solar cell performance. Elevated temperatures induce a shift in the characteristics of semiconductors, leading to a marginal rise in current and a significant fall in voltage. Extreme temperature increases may also shorten the operational lifetime of the module by causing damage to the cell and other materials. Since most of the heat produced by sunlight strikes cells, efficient thermal management extends the life of the cells.

II-9 IMPROVEMENT OF EFFICIENCY OF SOLAR PANEL USING DIFFERENT METHODS:

The efficiency of solar panels is dependent on a number of factors, including solar intensity (the more sunlight a solar cell can convert). The following techniques are applied to increase solar panel efficiency.

II-9-1 SUN TRACKER:

Trackers move in the direction of the sun or guide solar panels. In order to maximise energy capture, these devices rotate their orientation during the day to follow the course of the sun. Trackers in photovoltaic systems assist in reducing the angle of incidence between the incoming light and the panel, increasing the installation's energy output [25].

II-9-2 DUST CLEANING:

In order to ensure optimal performance, it is imperative to incorporate an auto cleaning system to eliminate dust particles from the panel's surface, as the electrical parameters of solar panels are very sensitive to dust density. One lesser-known issue that has a big impact on how well a PV installation performs is dust. Sunlight cannot reach the solar cells in your solar panels due to dust. The efficiency of solar panels may decrease due to dust [25].

II-9-3 ANTI REFLECTING COATING (ARC):

Solar energy packets are absorbed by the silicon cells upon light strike and transformed into electrical power. More than 35% of incident light is reflected away from the panel's surface before it can be transformed into useful energy due to the high refractive index of bare silicon [25].

The notion of "optical quarter wavelength" can help reduce reflection. The barrier layer between the antireflection medium and the silicon is where the penetrating light beam is reflected (figure II-12) [26].

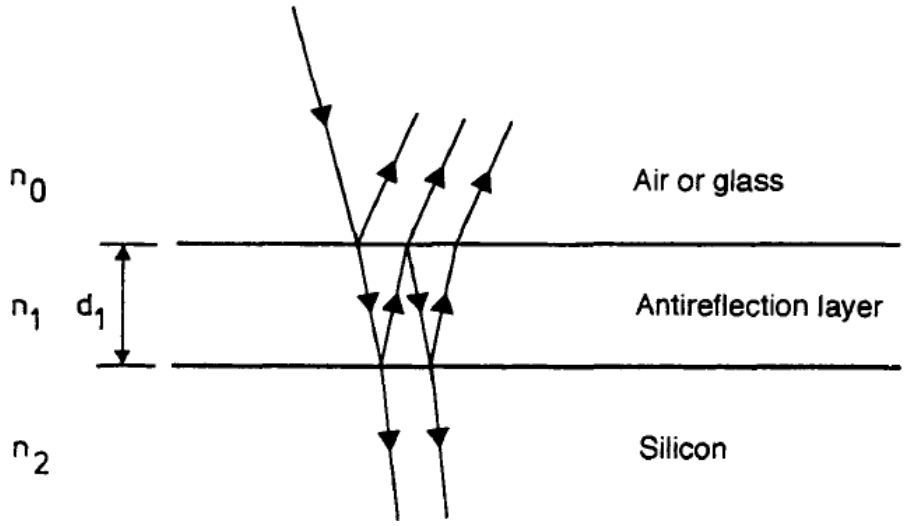

Figure (II-12): Antireflection behaviour of a thin film [26].

Owing to continuity conditions and conservation of energy, an electromagnetic wave undergoes a phase shift of $\pi / 2$ upon entry into an optically denser medium. If the thickness of the antireflection layer is chosen so that the optical path, i.e. the product of refractive index and layer thickness is equal to a quarter of the wavelength, then light of this wavelength falling vertically is completely extinguished (destructive interference). Written as a formula this condition reads:

$$n \times d = \frac{\lambda}{4} \qquad \textbf{(II-7)}$$

n : The product of refractive index.

d : Layer thickness.

λ : The wavelength.

II-9-4 COOLING TECHNIQUE:

High ambient temperatures and intense sun radiation can cause photovoltaic panels (PV) to overheat. The panels become less efficient when they overheat displays the optimal P–V characteristics of a solar cell for a temperature range of 0 °C to 75 °C (figure II-13). As the temperature of the solar cells rises, the maximum power output of the cells drops. This suggests that the PV panels' production may be considerably impacted by their heating [25].

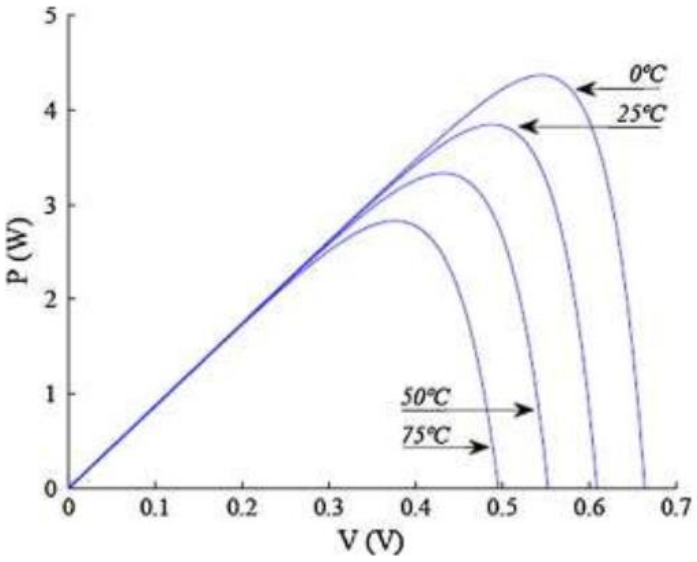

Figure (II-13): Surface temperature increment [25].

Hybrid Photovoltaic/Thermal (PV/T) solar system is one of the most popular methods for cooling the photovoltaic panels nowadays. The hybrid system consists of a solar photovoltaic panel combined with a cooling system. Water is circulated around the PV panels for cooling the solar cells, and the warm water leaving the panels pump back to water tank. Warm water mixed with cool water of tank [25].

II-10 TRANSPARENT CONDUCTING OXIDES (TCOs):

II-10-1 DEFINITION:

To finish the cell layout, TCO films were used to create contact between doped Si films and metallic elements. In solar cells, a TCO typically performs two functions:

1. the front TCO film serves as an anti-reflection coating and gathers charge carriers;
2. the rear TCO film functions as an electrode.

It was discovered that the short circuit current (J_{SC}) and fill factor (FF) in SCs are controlled by the refractive index, mobility, and extinction coefficient of TCO layers. In addition, a significant contribution to lowering the parasitic absorption losses in SCs is made by highly conductive TCO electrodes. Thus, a TCO layer with excellent optoelectrical characteristics is needed for the production of economical and efficient Si-based thin-film solar cells [27].

II-10-2 THEORY OF TCOs:

A metal oxide must transmit photons in the visible spectrum in order to be considered transparent. When a band gap (E_g) is greater than the energy of incoming photons in the visible spectrum (figure II-14), the material becomes transparent because the photons lack the energy necessary to excite the electrons from the valence band maximum (VBM) to the conduction band minimum (CBM)[28].

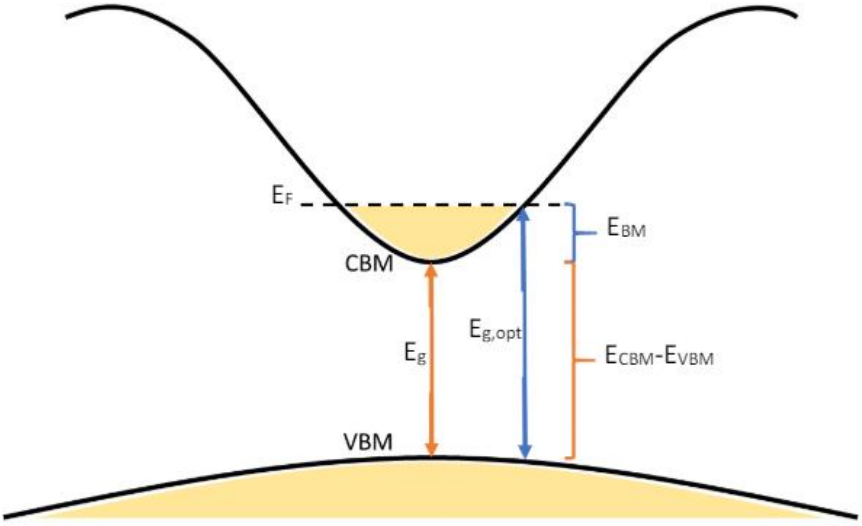

(Figure II-14): Overview of a direct band gap, E_g, with a Burnstein-Moss shift resulting in $E_{g,opt}$ [28].

A transparent metal oxide's band structure needs to be altered in order for it to also conduct. In order for electrons to conduct a current, they must be in states that are close to the CB, where transitions may be made with ease. In the case of thermal excitation at room temperature without an excess of electrons, E_g may be too big to sufficiently excite electrons to the CB where conduction would take place. However, when there is a surplus of electrons, more donor levels are produced near the CBM, making it possible to occupy states in the CB through thermal excitations [28].

$$E_g = E_{CBM} - E_{VBM} \qquad \textbf{(II-8)}$$

There are two basic ways to produce an excess of electrons: doping internally or doping externally. For example, oxygen vacancies in the metal oxide's lattice can be used to accomplish internal doping. By adding a higher valence atom in the lattice, external doping can be accomplished. Doping with an excess of electrons is known as n-doping, whereas doping with holes is known as p-doping. By n-doping, the optical band gap can shift, a so-called Burnstein-Moss shift. The lowest unoccupied state now lays higher up in the CB, the Fermi level (E_F) is shifted and the band gap expands. Now instead of to CBM being the optical band gap, it is now:

$$E_{g,opt} = E_{CBM} - E_{VBM} + E_{BM} \quad \textbf{(II-9)}$$

where E_{BM} is the Burnstein-Moss shift. The energy needed for a photon to excite an electron from the valence band is now increased.

II-10-3 ELECTRICAL CONDUCTIVITY:

TCOs are wide band gap (E_g) semiconducting oxides, with conductivity in the range 10^2 - 1.2×10^6 (S). The conductivity is due to doping either by oxygen vacancies or by extrinsic dopants. In the absence of doping, these oxides become very good insulators, with $\rho > 10^{10}$ Ω-cm. Most of the TCOs are n-type semiconductors. The electrical conductivity of n-type TCO thin films depends on the electron density in the conduction band and on their mobility [29].

$$\sigma = qn\mu \quad \textbf{(II-10)}$$

Where:

σ : is conductivity.

μ : is the electron mobility.

n : is the charge carrier density.

q : is the elementary charge ($1.602\times10^{-19} C$).

II-10-4 CHARACTERIZATION:

The transmittance and reflectance of a thin film are commonly used to characterise its optical characteristics. By using a monochromator to illuminate the sample at various wavelengths and measuring the amount of light that is transmitted or reflected, the parameters transmittance (T) and reflectance (R) can be determined. In order to determine the amount that was communicated or reflected, the system attempts to generate an ideal transmitting/reflecting sample, to which the actual sample is compared [29].

From the transmittance and reflectance values, the absorption (A) can be calculated with:

$$A = 1 - (R + T) \quad \textbf{(II-11)}$$

Resistivity is the primary parameter that characterises electrical qualities. The inversed conductivity can be used to determine the resistivity (ρ) of a film if the conductivity is known [29].

$$\sigma = \frac{1}{\rho} \qquad \textbf{(II-12)}$$

With a technique known as Four Point Probe (4PP), the resistivity of a film is determined by its sheet resistance. It consists of four points spaced one millimetre apart, the inner two of which measure the floating potential and the outside two of which are coupled to a direct current (figure II-15). The purpose of this configuration is to reduce the impact of contact resistance on the measurement [29].

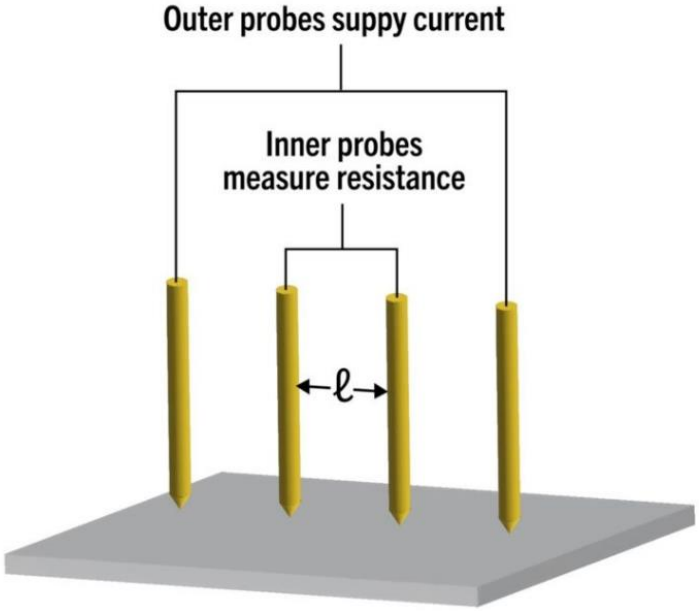

Figure (II-15): Schematic representation of the 4-point probe method for measuring the resistivity of a conductive band.

Equation (II-13) is used to obtain the conversion between the resistivity and the sheet resistance.

$$R_S = \frac{\rho}{d} \qquad \textbf{(II-13)}$$

where (d) is the thickness of the film.

II-10-5 TRANSPARENT CONDUCTING OXIDES APPLICATIONS :

TCOs are a game-changer in optoelectronics. They possess the magic touch of being both electrically conductive and transparent to light. This unique duo of properties opens doors to a variety of applications:

- **Solar Cells (PV):** Key component due to high transparency and conductivity. (ITO, ZnO…).
- **Flat Panel Displays (LCD, OLED):** Transparent electrodes for pixels. (ITO, AZO).
- **Touchscreens:** Transparent conducting layer for touch detection. (ITO).
- **Low-E Coatings (Windows):** Reflects infrared radiation for energy efficiency (ITO, ZnO…).
- **Other Potential:** Organic Photovoltaics, Solid-state Lighting (LEDs) Electrochromic Devices.

II-10-6 TITANIUM DIOXIDE:

William Gregor made the discovery of titanium (Ti), a transition metal with a silvery colour, in 1791. In the crust of the Earth, it is the seventh most prevalent metal and the ninth most abundant element [30]. Because of its strong affinities for oxygen, carbon, and nitrogen, titanium is a strong and light metal that is difficult to obtain in its pure state. Instead, it suffers from a phenomenon known as "passivation," which is the process of making a material "passive," usually by the deposition of an oxide layer that sticks to the metal surface [31].

Early in the 20th century, titanium dioxide was found, and in 1923, titanium white (anatase form) was first reported for use as a pigment in France. By the early 1930s, titanium white had completely replaced toxic lead-based pigments and lithopone. Three distinct crystallographic structures rutile, anatase, and brookite are found for TiO_2 [32].

II-10-6-1 TIO_2 STRUCTURAL PROPERTIES:

There are three crystalline forms of TiO_2: brookite, anatase, and rutile. Rutile has the lowest surface energy and is the most stable phase thermodynamically. It is more stable for anatase to be at low temperatures. Since it is difficult to make, there is no practical use for brookite. When heated over 600°C to 800°C, the metastable anatase and brookite phases permanently change into the rutile phase [33] (figure II-16).

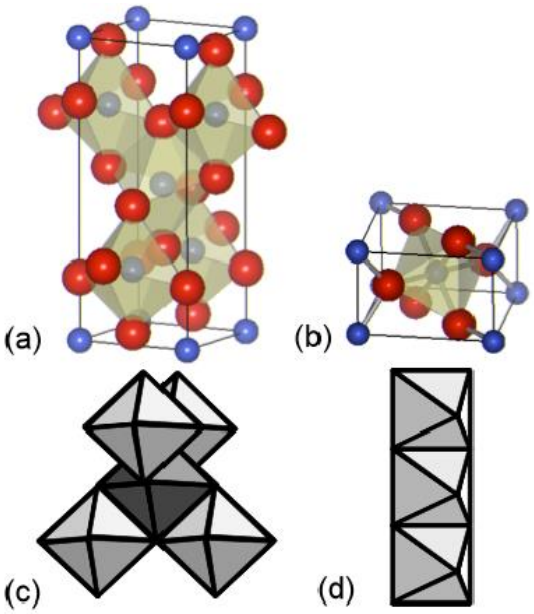

Figure (II-16): Crystal structures of (a) anatase and (b) rutile, and a schematic of the TiO_6 networks in (c) anatase and (d) rutile. Red and blue spheres denote Ti and O atoms, respectively [34].

In all three main crystal forms, each titanium (Ti) atom is bonded to six oxygen (O) atoms in an octahedral arrangement. These octahedra are then linked together in a specific way to form the overall crystal structure.

II-10-6-2 TIO_2 OPTICAL PROPERTIES:

In the visible spectrum, titanium dioxide has a high refractive index (n). Rutile has the greatest index (n = 2.66), greater than that of the anatase phase (n ≈ 2.54) among the three stable crystalline phases. This, along with a high visible light scattering coefficient, qualify the rutile phase for usage in the paint, food colouring, and pharmaceutical industries as a white pigment [35,36].

TiO_2 has good qualities such as UV protection, principal active component of solar cells, and high absorption in the ultraviolet due to its transparency in the visible range and absorption edge around 0.42 μm.

II-10-6-3 TiO_2 ELECTRICAL PROPERTIES:

A semiconductor of the n-type is titanium dioxide. At room temperature and 250 °C, the resistivity of a single TiO_2 crystal is around 10^7 Ω.cm and 10^{13} Ω.cm, respectively. These values are comparable to the $5\times10^{-14}\,\Omega^{-1}.cm^{-1}$ conductivity for a single crystal of rutile that was reported at 30 °C. It was reduced to $3.3\times10^{-9}\,\Omega^{-1}.cm^{-1}$ at 260 °C. As a result, TiO_2 is typically regarded as an insulator at temperatures lower than 200 °C and is employed in a variety of applications, including MOSFET devices' dielectric gates. But TiO_2 films electrical characteristics can be changed to make them highly conductive for a variety of uses, including gas sensors, photocatalysts, and solar cell contacts [37].

TiO_2 band structure is shown in (figure II-17) as can be observed. Wide band-gap semiconductors include TiO_2. The values of the gaps between the valence band (corresponding to the orbital O_{2p}) and the conduction band (corresponding to the Ti^{3d} orbital) for rutile, anatase, and brookite are 3 eV, 3.2 eV, and 3.1 eV, respectively. Transitions corresponding to photons in the ultraviolet region are produced by these gap values [38].

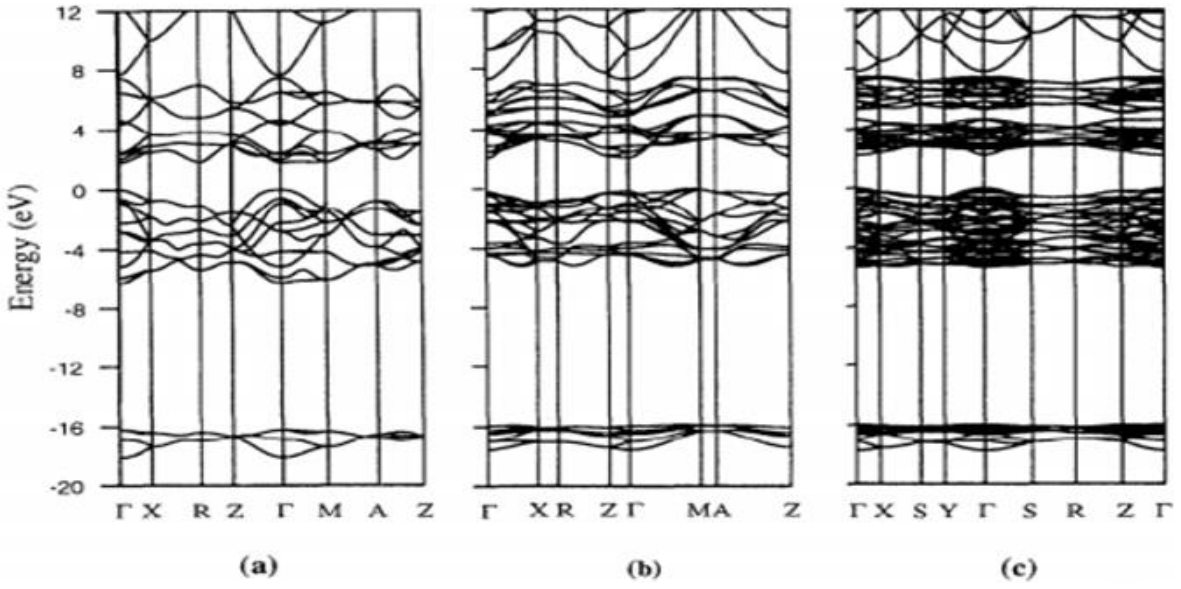

Figure (II-17): TiO_2 band structure for (a) rutile, (b) anatase and (c) brookite [39].

II-11 METAL-SEMICONDUCTOR HETEROJUNCTION:

The heterojunction is formed by the contact between two semiconductors with different gaps or between a metal and a semiconductor. At thermodynamic equilibrium the Fermi levels of the two materials align [40].

II-11-1 DEFINITION:

A metal-semiconductor junction is a structure that is formed when a metal is placed in contact with a semiconductor, called unipolar device, as the current is carried by a single type of carrier which is the electron or the hole. This structure contains one of the great number modern and complex electronic devices.

The energy band structure of the metal-semiconductor junction depends on the difference between the work functions of the metal $q\Phi_m$ and of the semiconductor $q\Phi_s$ as well as the doping of the semiconductor [40]. So, there are two types of contact which are: ohmic contact and rectifier contact, the type of contact depends on the output works of the materials.

II-11-1-1 OHMIC CONTACT:

When a contact occurs between the metal and the semiconductor, this contact can be ohmic. The electrons will diffuse towards the semiconductor or the metal depending on the type of the semiconductor until the alignment of the Fermi levels. The ohmic contact is characterized by a very low contact resistance, the electric current can easily pass through the junction in both directions and its characteristic I (V) will be linear.

II-11-1-2 RECTIFIER CONTACT:

When the contact is between the metal and the semiconductor is rectifier, the electrons will pass towards the semiconductor or the metal depending on the type of semiconductor until the alignment of the Fermi levels. The rectifier contact is characterized by the passage of the current in a specific direction and blocked in the other. The I (V) characteristic of this contact type has a rectifying behaviour.

II-11-2 METAL-SEMICONDUCTOR CONTACT:

Metal and semiconductor have different energy bands. When in contact, electrons move between the two materials to balance energy levels.

II-11-2-1 CASE WHERE $q\Phi_s = q\Phi_m$:

Before the contact, Fermi level of the metal E_{Fm} and of the semiconductor E_{Fs} are aligned because their distance on the level of the vacuum is the same.

When contact is made, the Fermi levels being already aligned, thermodynamic equilibrium is reached without exchange of electrons. In this case the energy bands are horizontal; this is called the flat band regime (figure II-18).

The potential barrier presented in the electrons which will pass from the metal to the semiconductor $q\Phi_b$ is given by:

$$q\Phi_b = q\Phi_m - q\chi_s \qquad \textbf{(II-14)}$$

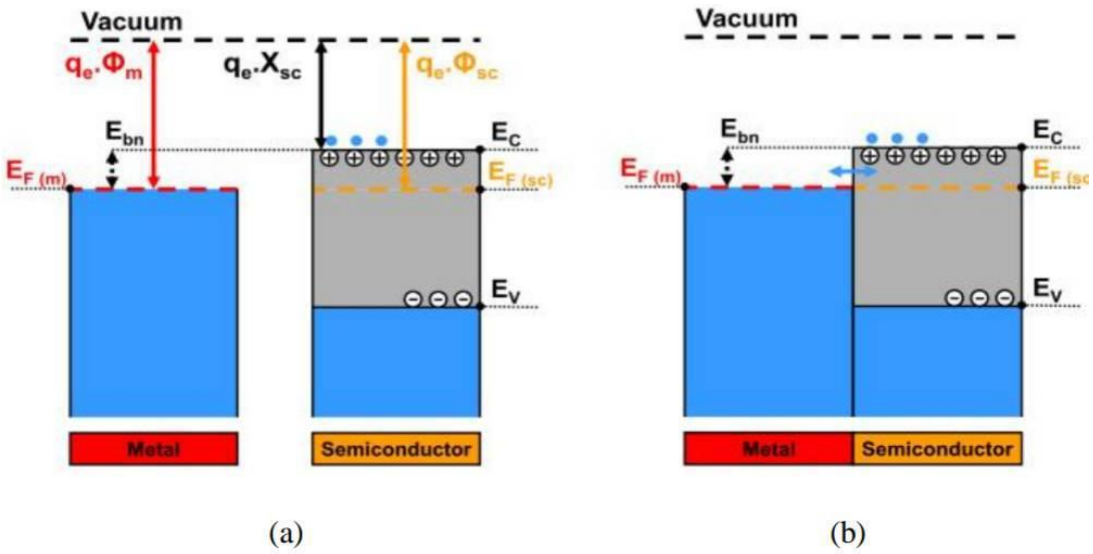

Figure (II-18): Energy band diagram of metal-semiconductor, when $q\Phi_s = q\Phi_m$,(a) before contact and (b) at thermodynamic equilibrium [41].

II-11-2-2 CASE WHERE $q\Phi_m > q\Phi_s$:

- **For n-type semiconductor:**

In this case, when bringing the metal and the semiconductor into contact, the electrons of the semiconductor have energy superior than those present in the metal, they will diffuse towards the metal until the alignment of Fermi levels, leaving behind fixed positive ions, to allow this alignment, the conduction and valence bands go down by $q\Phi_b$ (figure II-19)

$$q\Phi_b = q\Phi_m - q\chi_s \quad \textbf{(II-15)}$$

A deserted zone (ZCE) is formed which emptied of majority carriers appears in the semiconductor, due to the diffusion of electrons from the semiconductor to the metal, the majority carrier density is equal to the n doping of the semiconductor.

The height of the barrier which opposes the passage of electrons from the semiconductor to the metal is given by:

$$qV_b = q\Phi_m - q\Phi_s \quad \textbf{(II-16)}$$

V_b : Is the barrier potential of the ZCE.

A curvature of the energy bands upwards, since the Fermi level remains horizontal at thermodynamic equilibrium. On the metal side, at the interface, there remained an accumulation of electrons that have diffused from the semiconductor. The so-called "Schottky" contact, whose characteristic I (V) exhibits behaviour rectifier.

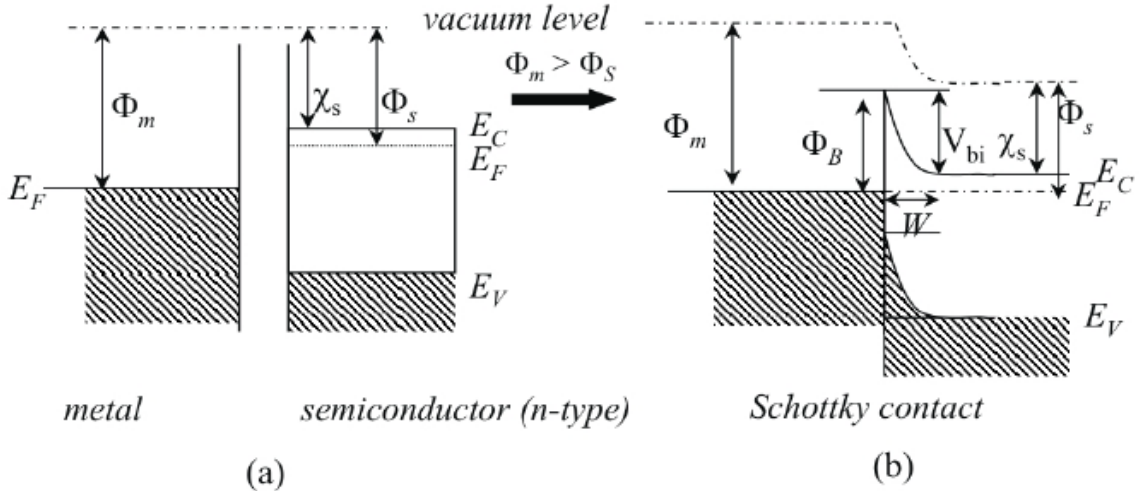

Figure (II-19): Energy band diagram of metal-n-type semiconductor contact when $q\Phi_m > q\Phi_s$, (a) before contact, (b) at thermodynamic equilibrium [42].

- **For p-type semiconductor:**

Electrons flow from semiconductor to metal to allow Fermi levels to line up, it appears at the interface, a zone of positive space charge (ZCE) in the semiconductor and a negative space charge on the metal side (an accumulation of electrons).

At the contact level, arrival or departure of a hole in the semiconductor is immediately compensated by the arrival or departure of an electron in metal. The contact is "ohmic" and has a characteristic I (V) linear and current flows freely in both directions (figure II-20).

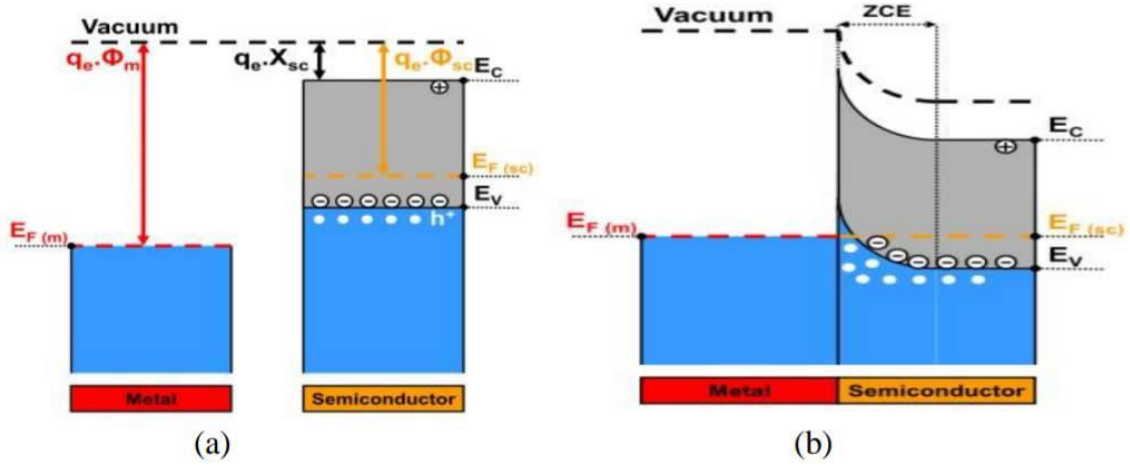

Figure (II-20): Energy band diagram of metal-p-type semiconductor contact when $q\Phi_m > q\Phi_s$, (a) before contact, (b) at thermodynamic equilibrium [41].

II-11-2-3 CASE WHERE $q\Phi_s > q\Phi_m$:

- **For n-type semiconductor:**

When bringing the metal and the semiconductor into contact, the electrons of the metal have energy superior than those present in the semiconductor, so they will diffuse towards the semiconductor (figure II-21).

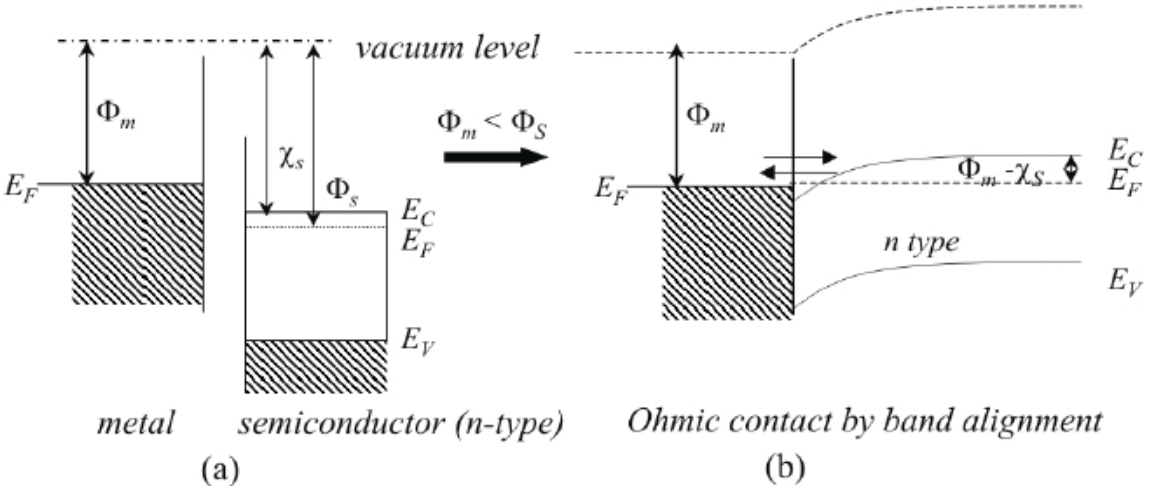

Figure (II-21): Energy band diagram of metal-n-type semiconductor contact when $q\Phi_m < q\Phi_s$, (a) before contact, (b) at thermodynamic equilibrium [42].

A zone of accumulation of free charge carriers (electrons) forms on the semiconductor side and a zone of deficit of negative carriers in the metal and the Fermi level align, it results in a curvature of the energy bands from the semiconductor to low energies, the contact is "ohmic" and has a characteristic I (V) linear.

- **For p-type semiconductor:**

The electrons of the metal will pass towards the semiconductor and recombine with the holes majority because of the difference in energy between them and it continues until an alignment of the Fermi level (figure II-22).

A zone of negative space charge forms on the semiconductor side and an electron deficiency at the interface on the metal side. Energy bands bend downward the diffusion barrier appears between the metal and the semiconductor and is given by the expression:

$$\Phi_b = (E_g - \Phi_m + \chi_s) \qquad \textbf{(II-17)}$$

In this case, the so-called “Schottky” contact, whose I (V) characteristic has a rectifying behaviour.

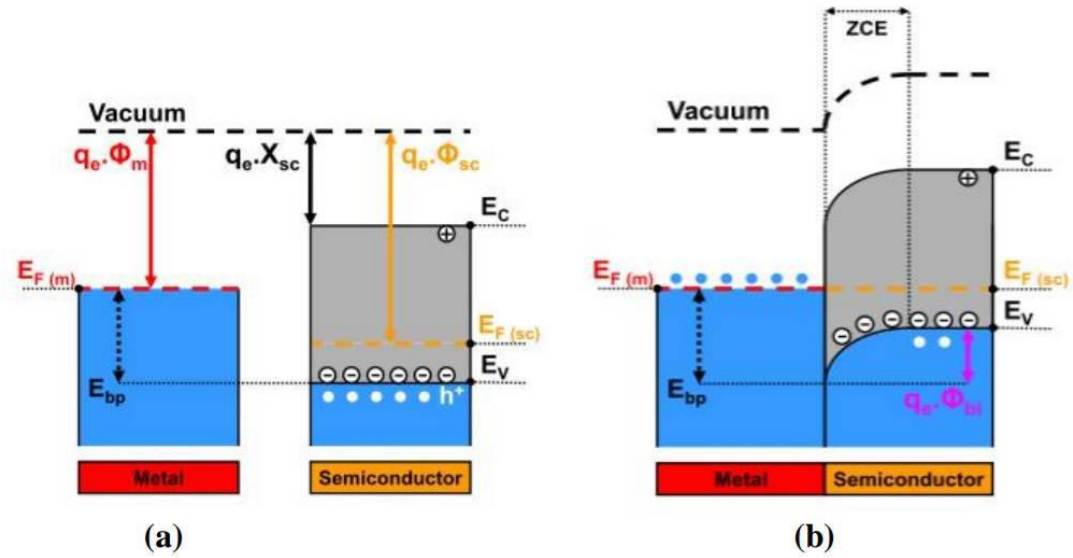

Figure (II-22): Energy band diagram of metal-p-type semiconductor contact when $q\Phi_m < q\Phi_s$, (a) before contact, (b) at thermodynamic equilibrium [41].

Table (II-1): different types of contact of metal semiconductor structure [40].

Contacts	n type semiconductor	p type semiconductor
Rectifier	$q\Phi_m > q\Phi_s$	$q\Phi_m < q\Phi_s$
ohmic	$q\Phi_m < q\Phi_s$	$q\Phi_m > q\Phi_s$

CHAPTER III: SIMULATION, RESULTS AND DISCUSSION

III-1 INTRODUCTION:

In this chapter we will focus on the simulation of solar cells to study TiO_2(n)-c-Si(p) and Zno(n)-c-Si(p) heterojunctions, using one-dimensional numerical simulation. We study the effect of:

- Transparent conductive oxides thickness,
- crystalline silicone layer thickness,
- carrier concentration of silicon,
- and carrier concentration of TCOs

on electrical properties under illumination conditions. In order to optimize the physical parameters for maximum efficiency. For this we used the AFORS-HET [1] simulation software (Automat FOR Simulation of HETerostructures).

The software AFORS-HET was used to conduct the simulation. Therefore, we provided an overview of the fundamentals of using this software to do a numerical simulation of the suggested cells, the extracted J-V characteristics, and the associated electrical output parameters.

III-2 PRESENTATION OF THE AFORS-HET SIMULATION SOFTWARE:

The laboratory Helmohlotz Zentrum Berlin (HZB) in Germany developed the AFORS-HET [1] software, a programme for one-dimensional (1D) numerical simulation that enables the simulation of semiconductor devices. Although this software can handle both homojunctions and heterojunctions, simulations of silicon-based heterojunction solar cells work especially well with it.

With the help of AFORS-HET [1]'s user-friendly graphical interface (figure III-1), you can quickly specify and construct a variety of structures, the majority of whose physical characteristics are controllable, including electron affinity, gap energy, mobility, doping, etc.

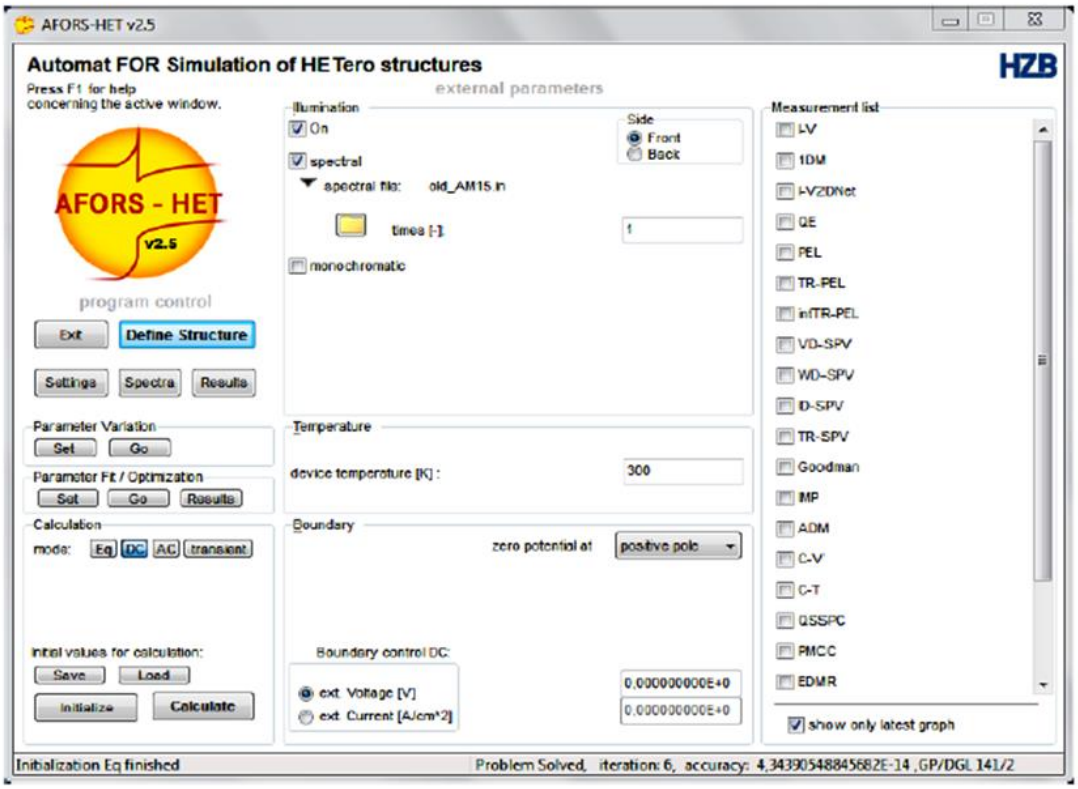

FIGURE (III-1): Graphical interface of the AFORS-HET simulation software.

This interface is primarily organised into three zones (figure III-2), each of them is dedicated to a specific role to achieve simulation. As follows:

- **First zone : program control**

This zone is used to specify both the structure to be simulated and the properties of each material employed. A structure consists of a front contact, a rear contact, and a number of layers separated by interfaces.

- **Seconde zone : External parameters**

This zone contains the external parameters, which are grouped into three categories: external temperature, spectrum illumination, and boundary conditions.

- **Third zone: Measurments**

This is where measurements are taken.

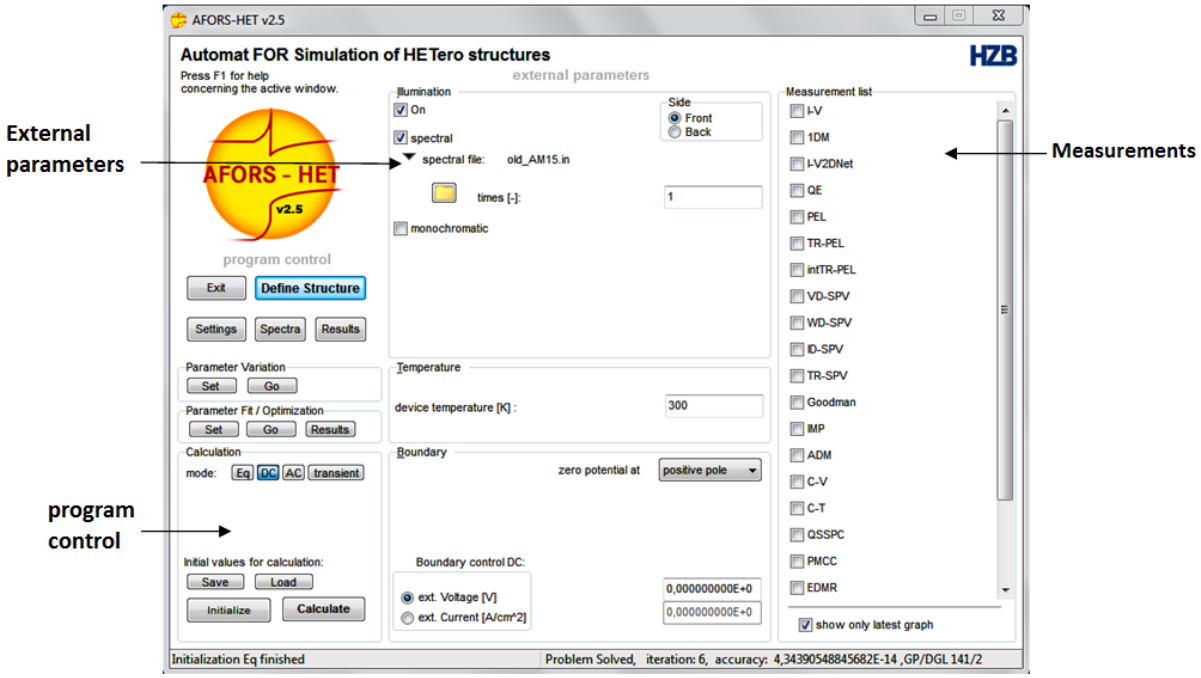

FIGURE (III-2): The three zones of the graphical interface.

III-3 SIMULATION STEPS:

We indicate the simulation steps as follows:

Using AFORS-HET [1], the initial step in the simulation process is to define the structure to be simulated. This structure is made up of a front contact, a back contact, and a configurable number of layers with interfaces in between. The following layers make up the structure that needs to be simulated:

- Front contact (The layer of TiO_2)
- Interface TiO_2 -Si(p))
- layer Si (p)
- A back contact.

It should be mentioned that during the structure definition, the numerical models at the layer interface will be defined.

The structure is defined first, and then each layer's parameters—such as thickness and electrical characteristics like doping and gap—are defined and introduced (figure III-3).

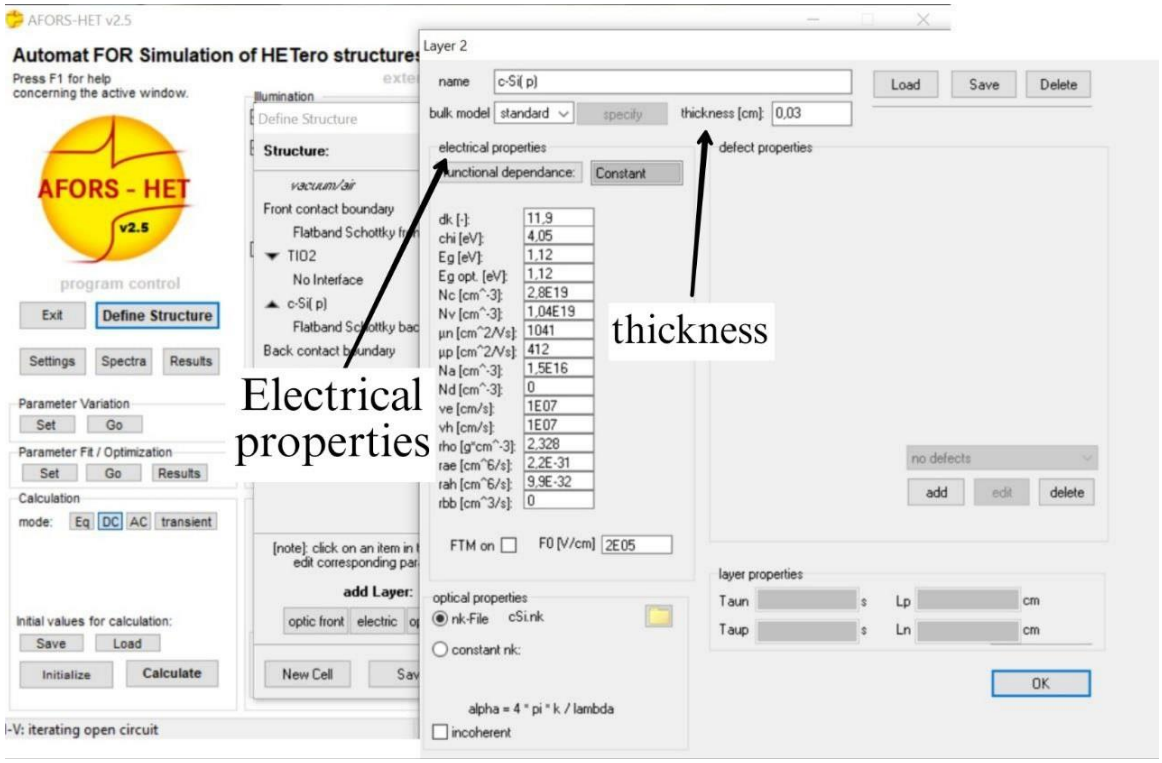

FIGURE (III-3): Definition of structure and introduction of parameters.

The thermodynamic equilibrium conditions are calculated when the structure is saved and built (figure III-4).

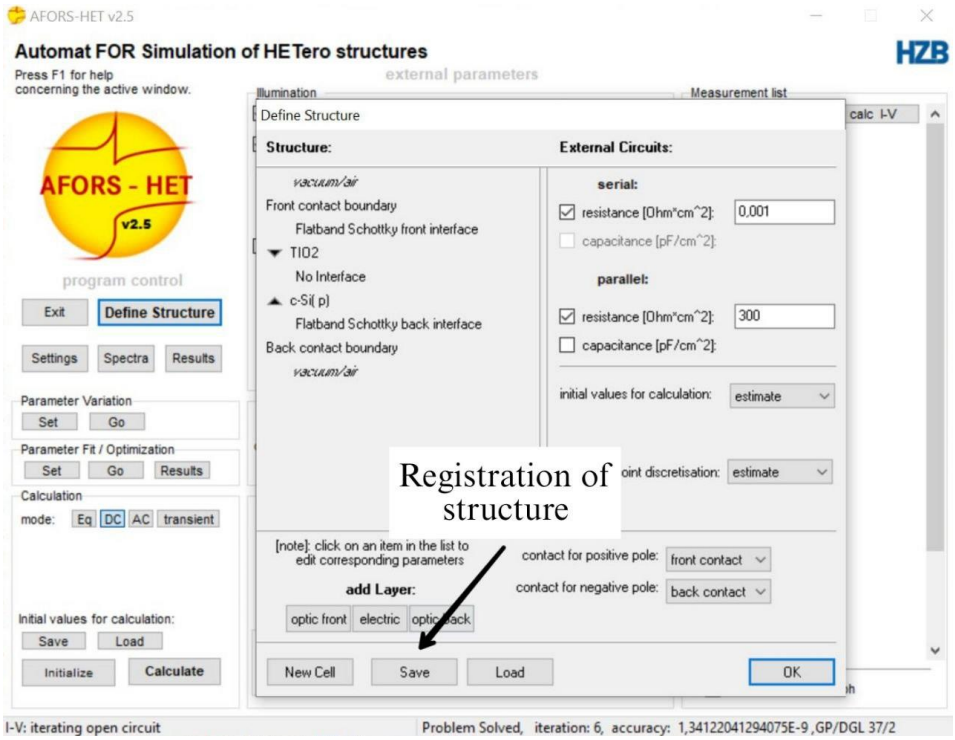

FIGURE (III-4): Registration of structure.

We first choose the AC polarisation mode or DC, and then choose the spectrum or monochromatic light with which we wish to operate (figure III-5).

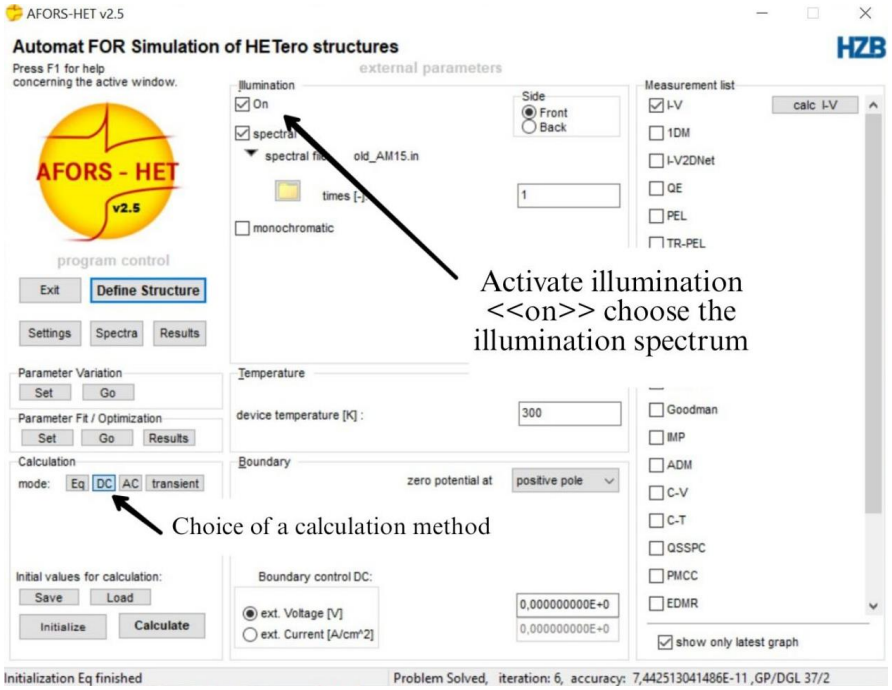

FIGURE (III-5): Calculation mode and illumination of the cell.

As a result, we are able to reproduce a wide range of experimental characterization methods (I-V, spectral response, photoluminescence spectrum, C-V, etc.).

III-4 THE PRESENTATION OF THE SIMULATED SOLAR CELL:

The structure of TiO_2(n)-c-Si(p) based heterojunction solar cell used in this simulation, is shown in figure III-6, it consists of an n-type TiO_2 (Titanium dioxide) layer used as emitter, and on top of main absorber p-type crystalline silicon substrate. This last layer is used as absorber. Thickness of the TiO_2 and p-Si layers has been taken as 0.06 µm and 300 µm, respectively.

The TiO_2 layer, in its capacity as TCO, plays a dual role: that of a conductive layer making it possible to conduct the charge carriers to the collection electrode and an antireflection layer making it possible to reduce the optical losses in the cell.

The structure was studied under solar spectrum AM1.5 with P = 1000 W/m^2 and T=300K. The measurements of the parameters were taken in the case of a parallel resistance R_P =300 Ω and a series resistor R_S =0.001 Ω.

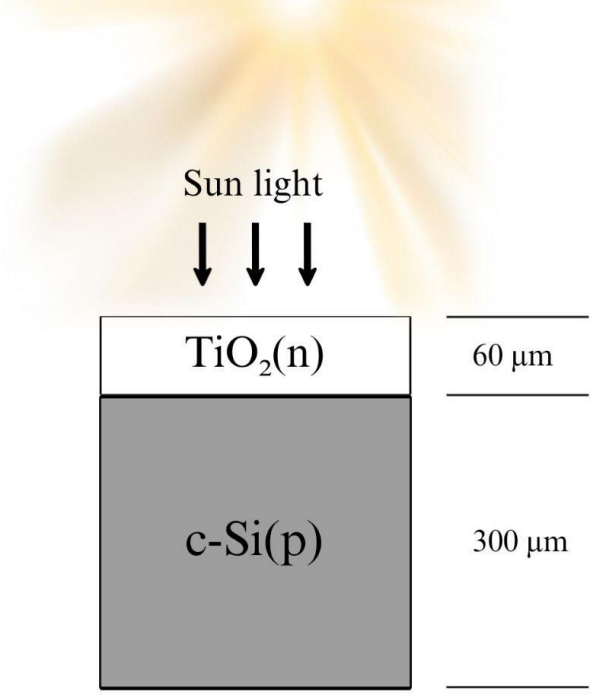

FIGURE (III-6): Schematic structure of TiO_2(n)-c-Si(p) heterojunction.

III-5 SIMULATION PARAMETERS:

The input parameters used in this simulation are given in the table below:

TABLE (III-1): Physical parameters used in the simulation.

Parameters	**TiO_2(n)**	**ZnO(n)**	**c-Si(p)**	**c-Si(n)**
Constant relative dielectric	8.6 [43]	9 [45]	11.9 [46]	11.9 [46]
Electron affinity χ (eV)	3.9 [43]	4.35 [45]	4.05 [46]	4.05 [46]
Energy gap (eV)	3 [43]	3.3 [45]	1.12 [46]	1.12 [46]
Effective density of states in the conduction band, N_C (cm^{-3})	1×10^{20} [44]	2.2×10^{8} [45]	2.8×10^{19} [46]	2.8×10^{19} [46]
Effective density of states in the valence band, N_V (cm^{-3})	1×10^{19} [43]	1.8×10^{19} [45]	1.04×10^{19} [45]	1.04×10^{19} [45]
Electron mobility, μ_n ($cm^2.V^{-1}.s^{-1}$)	20 [43]	100 [45]	1041 [46]	1041 [46]
Hole mobility, μ_p ($cm^2.V^{-1}.s^{-1}$)	10 [43]	25 [45]	412 [46]	412 [46]
Concentration of acceptor atoms, N_a (cm^{-3})	0	0	1.5×10^{16} [46]	0
Concentration of donor atoms, N_d (cm^{-3})	1×10^{17} [44]	7×10^{19} [45]	0	1.5×10^{16} [46]
Thermal velocity of electrons, V_e ($cm.s^{-1}$)	2.99×10^{6} [43]	10^{7} [45]	10^{7} [46]	10^{7} [46]

Thermal velocity of holes, V_h (cm.s^{-1})	6.76×10^{6} [43]	10^{7} [45]	10^{7} [46]	10^{7} [46]
Layer density, *rho* (g.cm^{-3})	2.328 [43]	5.606 [45]	2.328 [46]	2.328 [46]
Layer thickness (cm)	6×10^{-6}	6×10^{-6}	0.03	0.03

III-6 SIMULATION RESULTS:

III-6-1 CURRENT-VOLTAGE CHARACTERISTIC OF TiO_2(n)/c-Si(p) SOLAR CELL:

The J-V characteristic of the TiO_2(n)-c-Si(p) solar cell simulated by AFORS-HET is shown in figure III-7.

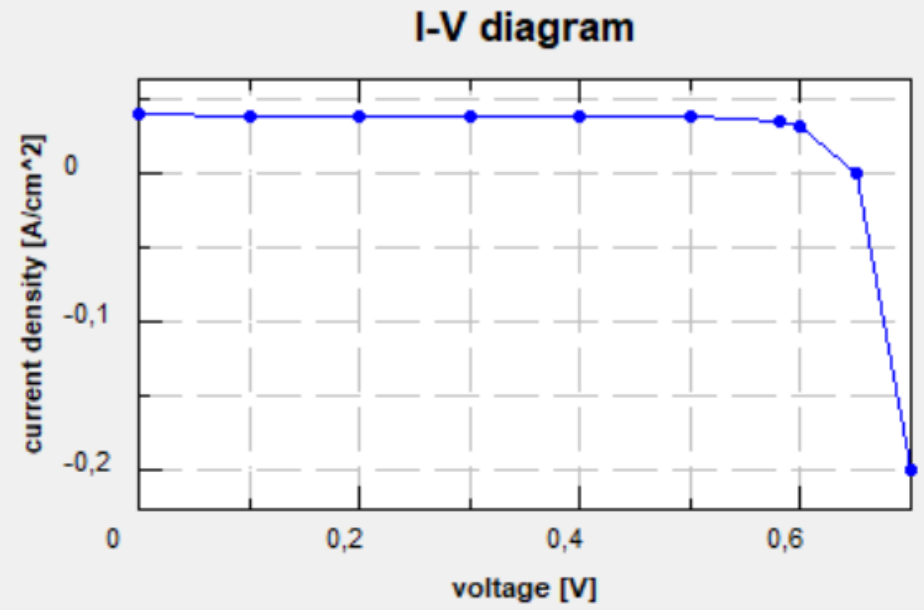

FIGURE (III-7): J-V characteristic of TiO_2(n)-c-Si(p) solar cell.

Solar Cell I-V Characteristic Curves are graphs that represent the variation of the current as a function of the voltage for different levels of insulation and temperature that means the operation of photovoltaic cells depends on the conditions of sunlight and the temperature at the surface of the cell.

Current density (J) represents the amount of current flowing through a given area, the relationship between current (I) and current density (J) can be expressed as follows:

$$J = \frac{I}{A} \qquad \textbf{(III-1)}$$

J : is the current density (measured in amperes per square meter, A/m²).

I : is the current (measured in amperes, A).

A : is the cross-sectional area through which the current is passing (measured in square meters, m²).

The curve obtained in this study, is the characteristic curve J(V) of the TiO_2/Si(p) solar cell type (figure III-7). This characteristic curve represents the variation of the electric current density (J) with the applied voltage (V) to the solar cell for specific operating conditions. The current density-voltage relation of heterojunction is usually written as a function of the applied voltage (V) as described in the following equation:

$$J = J_S\left[e^{\left(\frac{qV}{nKT}\right)} - 1\right] - J_{SC} \qquad \textbf{(III-2)}$$

The J(V) characteristic curve provides a clear reading of the photovoltaic constants that characterize the solar cell which are:

- **The short circuit current density J_{SC} :**

The current density intensity generated by the solar cell when the voltage across it is zero and represents the maximum current density that the cell can output under a certain light intensity.

- **The open ‑circuit voltage V_{OC} :**

The open circuit voltage is achieved when there is no current flowing through the solar cell. It represents the maximum voltage that the cell can reach under a given level of illumination.

- **Fill factor FF :**

The fill factor, also known as the form factor, is defined as the ratio between the maximum power supplied by the solar cell ($P_{\max}$) and the product of the short-circuit current (I_{SC}) and

the open-circuit voltage (V_{OC}). It serves as an indicator of the electrical performance of the cell and can provide insights into the cell's aging characteristics.

- **Efficiency η:**

It is defined as the ratio between the maximum power received by the solar cell and the intensity of the incident light. This efficiency value is crucial as it allows for the evaluation of cell performance and facilitates comparisons between different solar cells.

The values of these photovoltaic constants for our study are grouped in Table III-2:

Table (III-2): Electrical parameters of simulated TiO_2(n)-c-Si(p) solar cell.

Parameters	V_{OC} (mV)	J_{SC} (mA /cm^2)	FF (%)	η (%)
TiO_2(n)-c-Si(p)	650.8	38.86	78.98	19.97

III-6-2 CURRENT-VOLTAGE CHARACTERISTIC OF ZnO(n)/c-Si(p) SOLAR CELL:

The J-V characteristic of the ZnO(n)-c-Si(p) solar cell simulated by AFORS-HET is shown in figure III-8.

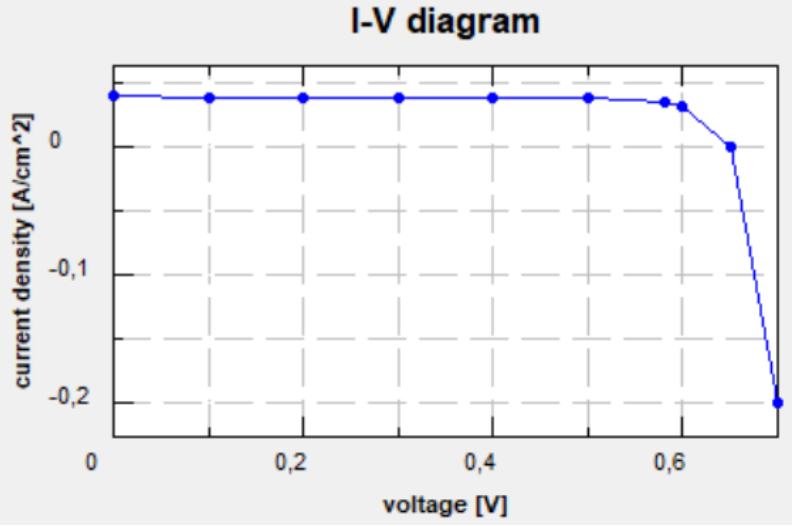

FIGURE (III-8): J-V characteristic of ZnO(n)-c-Si(p) solar cell.

The values of these photovoltaic constants for our study are grouped in Table III-3:

Table (III-3): Electrical parameters of simulated ZnO(n)-c-Si(p) solar cell.

Parameters	V_{OC} (mV)	J_{SC} (mA /cm^2)	FF (%)	η (%)
ZnO(n)-c-Si(p)	650.8	38.64	78.92	19.84

III-7 PARAMETERS INFLUENCING THE PERFORMANCE OF SOLAR CELLS:

III-7-1 EFFECT OF c-Si(p) THICKNESS:

III-7-1-1 TiO_2(n)/c-Si(p) :

In this section, we begin an optimization of c-Si(p) thickness in order to obtain the most evident thickness to determine the structure that consuming less energy. For that, we are simulated the current-voltage characteristics for different c-Si(p) thickness at a fixed charge carrier concentration. So, we study the thickness effect of the Si(p) layer on the solar cell efficiency (figure III-9). The layer thickness is varied from 40 µm to 300 µm.

Table (III-4): Effect of p-layer (c-Si) thickness on electrical output parameters.

Thickness (μm)	40	100	200	250	300
V_{OC} (mV)	593	619.5	639.8	646.1	650.8
J_{SC} (mA /cm^2)	31.65	35.49	37.74	38.37	38.86
FF (%)	77.1	75.36	73.51	72.91	78.98
η (%)	14.47	16.57	17.75	18.08	19.97

Through table (III-4) and the curve of (figure III-9), it is seen that the efficiency increases slightly with increasing the thickness of the c-Si(p) layer. This is due to the increase of the number of the pairs (electron- hole), which rise with the evolution of the layer volume.

The use of a thicker substrate, specifically 300 µm (in our case), has a good effect on improving the efficiency value.

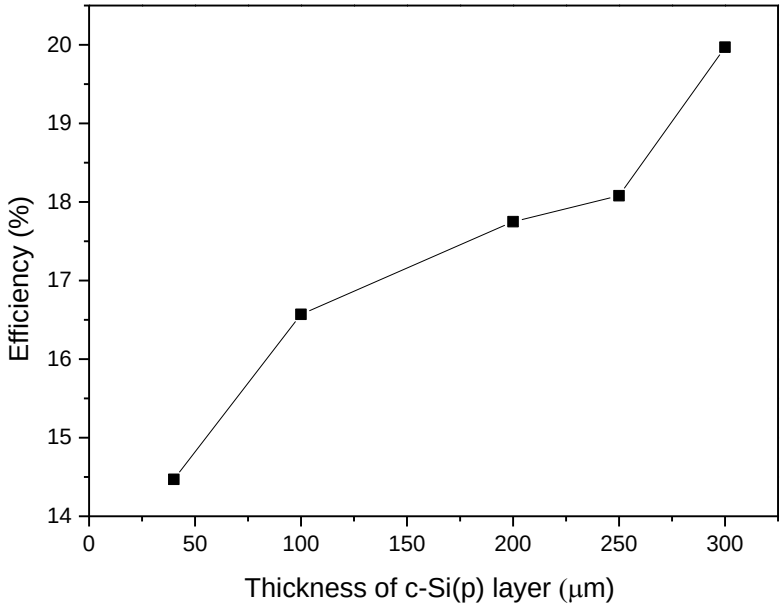

Figure (III-9): Efficiency variation depending on the thickness of c-Si (p).

The increase of the cell conversion efficiency can be attributed to an increase in both the open circuit voltage and the short circuit current. This relationship is demonstrated by the following:

$$\eta = \frac{V_m I_m}{P_{inc}} = FF \frac{V_{OC} I_{SC}}{P_{inc}} \qquad \textbf{(III-3)}$$

P_{inc} : Incident power.

III-7-1-2 ZnO(n)/c-Si(p):

we are simulated the current-voltage characteristics for different c-Si(p) thickness at a fixed charge carrier concentration. We study the thickness effect of the c-Si(p) layer on the solar cell efficiency (figure III-10). The layer thickness is varied from 40 μm to 300 μm.

Table (III-5): Effect of p-layer (c-Si) thickness on electrical output parameters.

Thickness (μm)	40	100	200	250	300
V_{OC} (mV)	593	619.5	639.8	646.1	650.8
J_{SC} (mA /cm^2)	31.47	35.3	37.53	38.16	38.64

FF (%)	77.04	75.33	73.48	72.89	78.92
η (%)	14.38	16.47	17.65	17.97	19.84

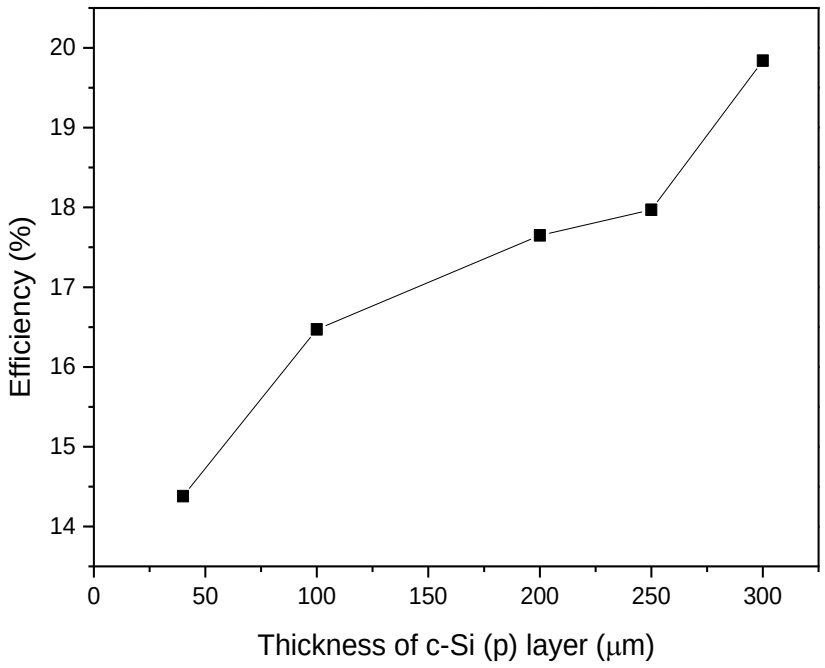

Figure (III-10): Efficiency variation depending on the thickness of c-Si (p).

Through table (III-5) and the curve of (figure III-10), it is seen that the efficiency increases slightly with increasing the thickness of the c-Si(p) layer. This is due to the increase of the number of the pairs (electron- hole), which rise with the evolution of the layer volume.

The use of a thicker substrate, specifically 300 μm (in our case), has a good effect on improving the efficiency value.

The increase of the cell conversion efficiency can be attributed to an increase in both the open circuit voltage and the short circuit current.

III-7-2 EFFECT OF TCO THICKNESS:

III-7-2-1 TiO_2(n)/c-Si(p) :

We study the thickness effect of the n-TiO_2 layer on the solar cell efficiency (fig III-11). The layer thickness is varied from 60 nm to 590 nm.

Table (III-6): Photovoltaic parameters of TiO_2(n)-Si(p) solar cell with different thickness value of TiO_2.

Thickness (*nm*)	60	150	360	480	590
V_{OC} (mV)	650.8	650.8	650.8	650.8	650.8
J_{SC} (mA /cm^2)	38.86	38.86	38.86	38.86	38.86
FF (%)	78.98	78.98	78.98	78.98	78.98
η (%)	19.97	19.97	19.97	19.97	19.97

The table III-5 shows the effect of TiO_2(n) thickness on the short circuit current density, the open circuit voltage, form factor and efficiency. Based on the obtained results, it has been observed that the efficiency has a constant value. So, the best performance and highest efficiency of the TiO_2(n)-c-Si(p) solar cell is depended on the c-Si(p) layer only.

III-7-2-2 ZnO(n)/c-Si(p) :

We study the thickness effect of the ZnO(n) layer on the solar cell efficiency (fig III-11). The layer thickness is varied from 60 nm to 590 nm.

Table (III-7): Photovoltaic parameters of ZnO(n)-Si(p) solar cell with different thickness value of ZnO(n).

Thickness (*nm*)	60	150	360	480	590
V_{OC} (mV)	650.8	650.8	649.2	649.2	649.2
J_{SC} (mA /cm^2)	38.64	38.3	37.51	37.08	36.68
FF (%)	78.92	78.83	78.8	78.68	78.56
η (%)	19.84	19.65	19.19	18.94	18.71

The table III-7 shows the effect of ZnO(n) thickness on the short circuit current density, the open circuit voltage, form factor and efficiency.

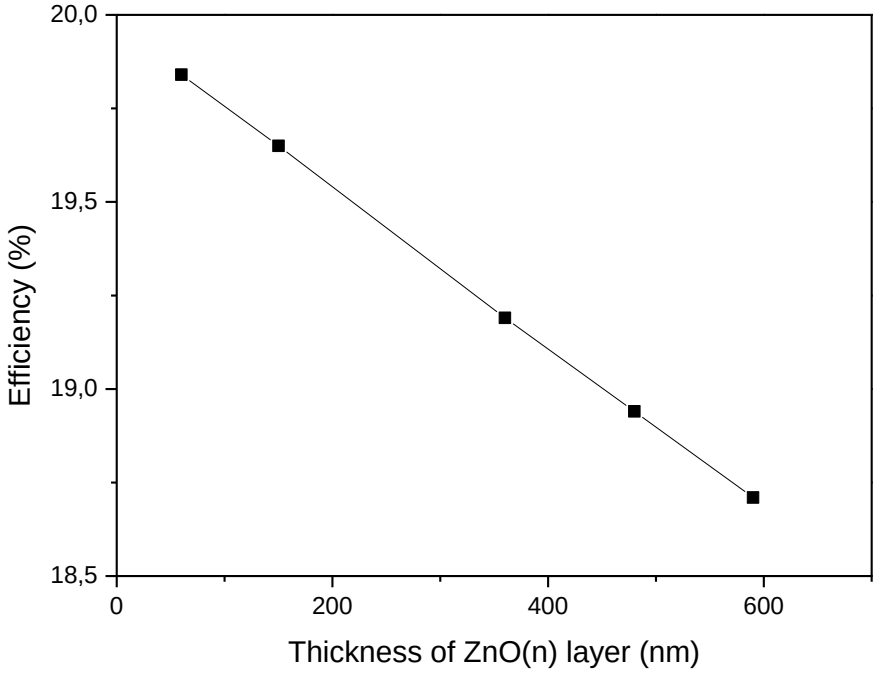

Figure (III-11): Efficiency variation depending on the thickness of ZnO(n).

Based on the obtained results, it has been observed that the solar cell exhibits the best performance and highest efficiency when the ZnO(n) layer has a thickness of 60 *nm* .It is noted that increasing the thickness of this layer results in a decrease in the short-circuit current, which consequently leads to a decrease in the overall efficiency. This is due to the absorption of the UV light by the ZnO(n) materials. As the thickness of the ZnO(n) layer increases, a larger portion of the incident UV photons is absorbed within the ZnO(n) layer itself. Consequently, some photons reach the space charge zone where the photoelectric conversion takes place.

This reduction in the number of photons reaching the space charge region leads to a decrease in the overall current generated by the solar cell, resulting in a lower efficiency; this is consistent with the previous study shown in the table III-7.

III-7-3 EFFECT OF SILICON DOPING:

III-7-3-1 TiO_2(n)/c-Si(p) :

we aim to investigate the impact of silicon doping on the photovoltaic parameters of a TiO_2(n)-c-Si(p) solar cell. We will vary the doping concentration of silicon within the range of 1×10^{16} to 3×10^{16} cm^{-3}. By altering the doping level, we can assess how it affects the performance of the solar cell and its photovoltaic parameters.

Table (III-8): Photovoltaic parameters of TiO_2(n)-c-Si(p) solar cell with different doping value of c-Si(p).

Doping (cm^{-3})	1×10^{16}	1.5×10^{16}	2×10^{16}	2.5×10^{16}	3×10^{16}
V_{OC} (mV)	639.8	650.8	658.6	664.8	669.5
J_{SC} (mA /cm^2)	38.46	38.86	39.2	39.51	39.79
FF (%)	73.58	78.98	79.59	79.77	79.7
η (%)	18.11	19.97	20.55	20.95	21.23

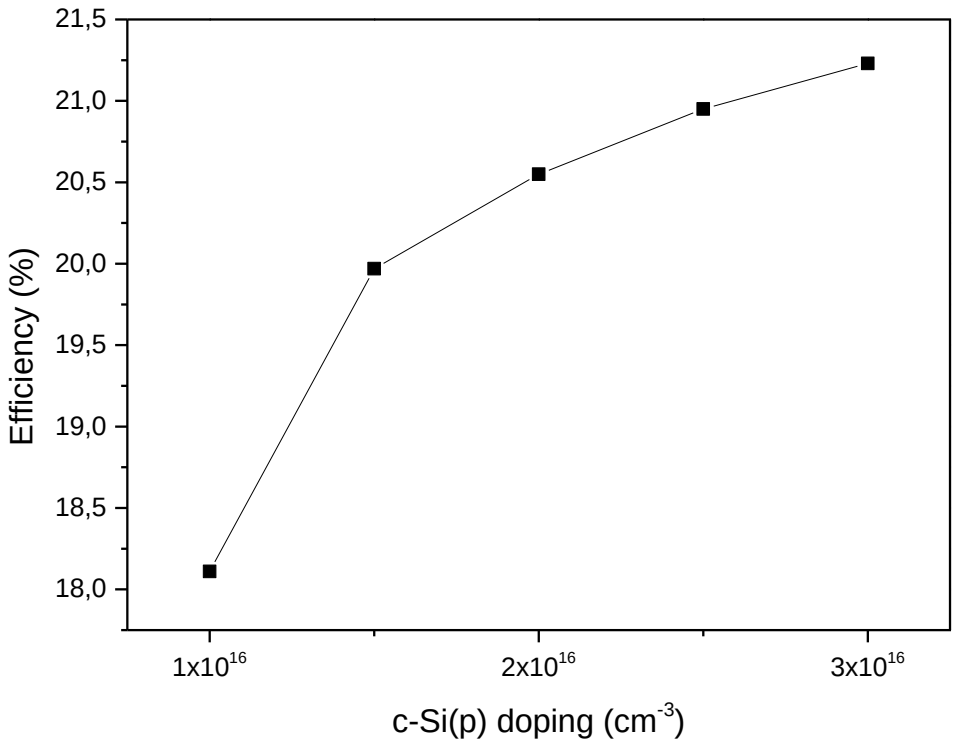

Figure (III-12): Efficiency variation depending on the doping of c-Si(p).

The carrier concentration of 3×10^{16} cm^{-3} gives the best performance, according to the results collected in table III-8 and (figure III-12). Consequently, we can say that using a highly doped silicon layer allows for a significant increase in efficiency because the potential barrier

height between the semiconductor and the Transparent conductive oxide (TCO) layer is directly impacted by variations in silicon doping concentration.

III-7-3-2 ZnO(n)/c-Si(p) :

Our goal in this work is to examine how silicon doping affects a ZnO(n)-c-Si(p) solar cell's photovoltaic characteristics. We will vary the doping concentration of silicon within the range of 1×10^{16} to 3×10^{16} $cm^{-3.}$ We may evaluate how the doping level impacts the photovoltaic parameters and solar cell performance by varying it.

Table (III-9): Photovoltaic parameters of ZnO(n)-c-Si(p) solar cell with different doping value of c-Si(p).

Doping (cm^{-3})	1×10^{16}	1.5×10^{16}	2×10^{16}	2.5×10^{16}	3×10^{16}
V_{OC} (mV)	639.8	650.8	658.6	663.3	669.5
J_{SC} (mA /cm^2)	38.26	38.64	38.96	39.24	39.49
FF (%)	73.55	78.92	79.54	79.9	79.63
η (%)	18.01	19.84	20.41	20.8	21.05

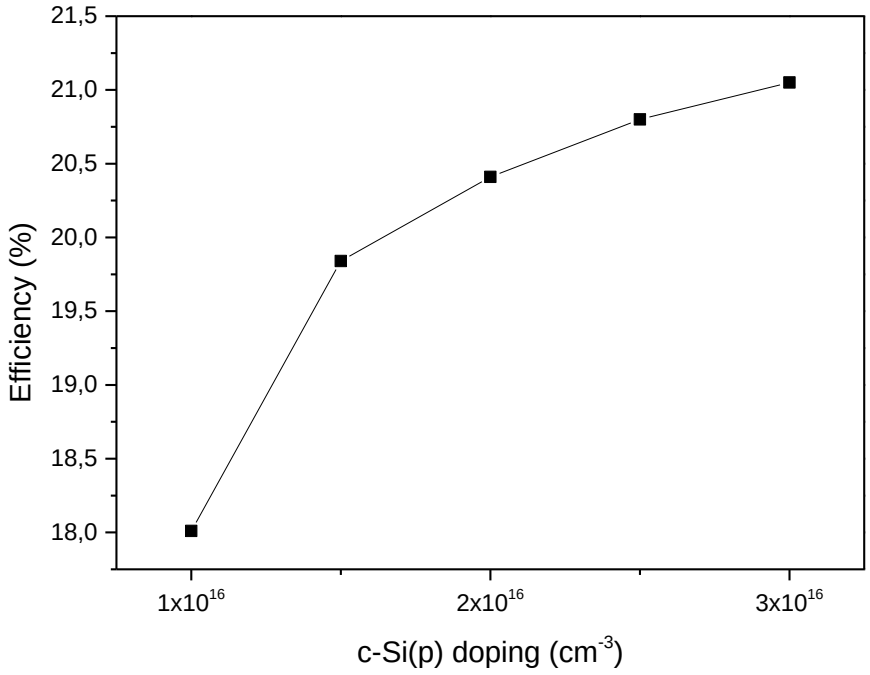

Figure (III-13): Efficiency variation depending on the doping of c-Si(p).

From the results summarized in table III-9 and (figure III-13), the best performance is obtained with the carrier concentration equal to 3×10^{16} cm^{-3}. As a result, we can conclude that the use of highly doped silicon layer, allows a considerable increase in the efficiency, because the variation in the doping concentration of silicon has a direct influence on the height of the potential barrier between the semiconductor and the Transparent Conductive Oxide (TCO) layer.

III-7-4 EFFECT OF TCOs DOPING:

III-7-4-1 TiO_2(n)/c-Si(p):

We keep all simulation values constant while changing the doping of titanium dioxide from 1×10^{16} to 1×10^{20}.

Table (III-10): Photovoltaic parameters of TiO_2(n)-c-Si(p) solar cell with different doping value of TiO_2(n).

Doping (cm^{-3})	1×10^{16}	1×10^{17}	1×10^{18}	1×10^{19}	1×10^{20}
V_{OC} (mV)	650.8	650.8	650.8	650.8	650.8
J_{SC} (mA /cm^2)	39.2	38.86	38.77	38.74	38.72
FF (%)	78.99	78.98	78.96	78.95	78.94
η (%)	20.15	19.97	19.92	19.9	19.89

We conclude that increasing TiO_2 doping negatively affects solar cell performance because the results, as summarised in table III-10 and (figure III-14), show that cell efficiency gradually decreases with decreasing doping from a maximum of 20.15%. This decrease is significant in the range of 1×10^{16} to 1×10^{20}. After reaching the value of 19.92%, it continues to decrease by a small amount until it reaches 19.89%.

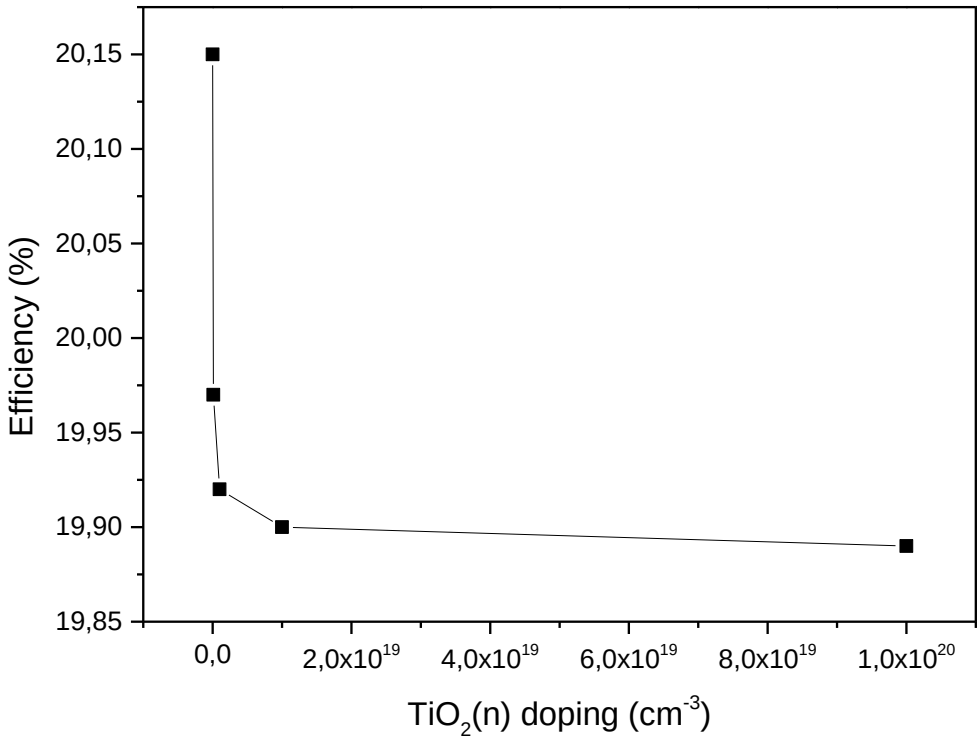

Figure (III-14): Effect of titanium dioxide doping on heterojunction TiO_2(n)/c-Si(p) efficiency.

III-7-4-1 ZnO(n)/c-Si(p):

We keep all simulation values constant while changing the doping of zinc oxide from 7×10^{18} to 7×10^{22}

Table (III-11): Photovoltaic parameters of ZnO(n)-c-Si(p) solar cell with different doping value of ZnO(n).

Doping (cm^{-3})	7×10^{18}	7×10^{19}	7×10^{20}	7×10^{21}	7×10^{22}
V_{OC} (mV)	650.8	650.8	650.8	650.8	650.8
J_{SC} (mA /cm^2)	38.67	38.64	38.61	38.59	38.56
FF (%)	78.92	78.92	78.91	78.91	78.9
η (%)	19.86	19.84	19.83	19.81	19.8

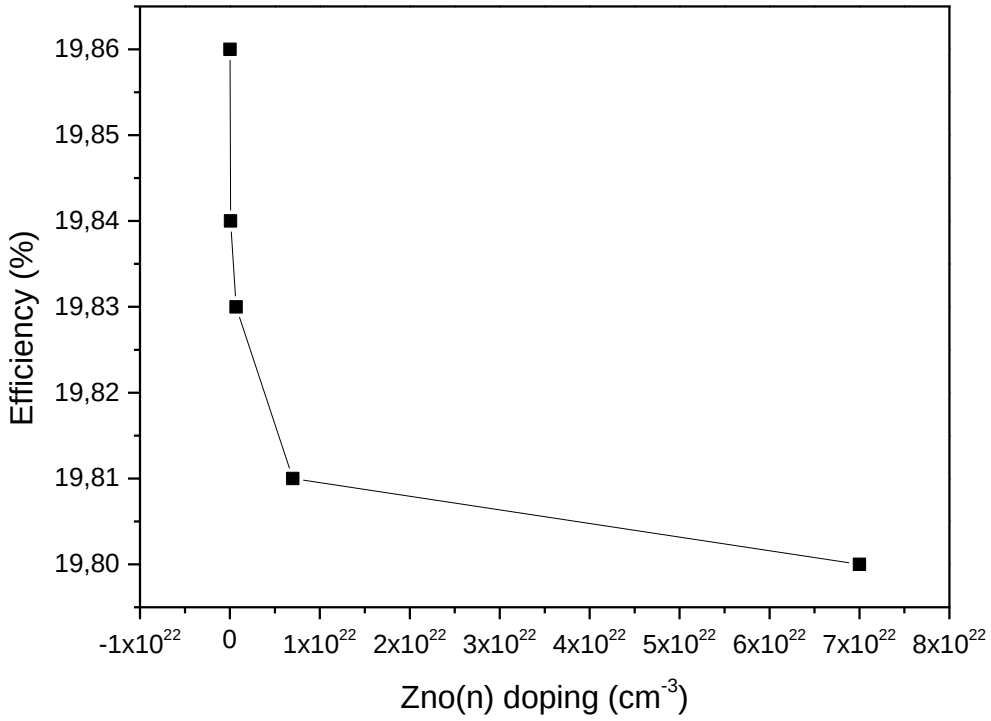

Figure (III-15): Effect of zinc oxide doping on heterojunction TiO_2(n)/c-Si(p) efficiency.

From the results summarized in Table III-11 and (figure III-15), we observe that cell efficiency decreases gradually with decreasing of doping from a maximum 19.86 % and this decrease is be significantly in the range 7×10^{18} to 7×10^{22}. It continues to decrease by a small amount until it reaches to 19.8%, We conclude that increasing doping of ZnO adversely affects the performance of the solar cell.

GENERAL CONCLUSION

In this work, we present a theoretical study of the heterojunction solar cells. We focus more on the transparent conductive oxides TCOs. For this we choose the TiO_2(n)-c-Si(p) and ZnO(n)-c-Si(p) heterojunction solar cells and we study these structures with the Afors-het (Automate for Simulation of heterostructures) software [1].

We use the titanium dioxide (TiO_2) as the transparent electrode in our studied solar cell. We choose it for its good electrical conductivity in one way. In the other way, this oxide acts as an anti-reflective because of its high transparency in the visible and near-infrared spectral range.

In this simulation, we study the impact of the doping of each layer, TCOs represented by TiO_2 and ZnO thicknesses and silicon thickness on the performances of the TiO_2(n)-c-Si(p) and ZnO(n)-c-Si(p) heterojunction solar cells, that means its effect on the electrical parameters of the solar cell. The electrical parameters are: short-circuit current density J_{SC} (mA/cm2), open circuit voltage V_{OC} (mV), fill factor FF (%) and the efficiency η (%) in order to obtain a device with good conversion efficiency.

The simulation results obtained shows that each change in the parameters studied (doping, thickness) has an influence on the cell's performance. First, we simulated this solar cell under AM 1.5 illumination and for a TiO_2 and ZnO thicknesses of 6×10^6 nm and a silicon thickness of 0.03 cm. For these input parameters, we obtain the following results: a short circuit current density of 38.86 mA/cm², an open circuit voltage of 650.8 mV, a fill factor of 78.98%, and a photovoltaic conversion efficiency of 19.97 % for TiO_2(n)-c-Si(p) and a short circuit current density of 38.64 mA/cm², an open circuit voltage of 650.8 mV, a fill factor of 78.92%, and a photovoltaic conversion efficiency of 19.84 % for and ZnO(n)-c-Si(p). The best conversion efficiency is 21.23% with TiO_2 and 21.05% with ZnO. We achieve these results with $N_A=3\times10^{16}$ cm^{-3}, substrate of Si of 0.03 cm, $N_D=1\times10^{17}$ cm^{-3}, emitter (TiO_2) thick 6×10^{-6} cm and $N_A=3\times10^{16}$ cm^{-3}, substrate of Si 0.03 cm, $N_D=7\times10^{19}$ $cm^{-}3$, emitter (ZnO) thick 6×10^{-6} cm respectively.

Finally, through our work, we conclude that the increase of both doping and thickness of the silicon layer lead to an increase in cell efficiency. However, the increasing of the TiO_2 and ZnO layer thickness and doping reduced the efficiency of our solar cell. It should be noted that this conclusion relates only to the range used in this simulation.

REFERENCES

[1] S. Stangl, A. Froitzheim, M. Kriegel, T. Brammer, S. Kirste, L. Elstner, H. Stiebig, M. Schmidt, W. Fuhs,
"AFORS-HET, a numerical PC-program for simulation of heterojunction solar cells, version 1.1" Proc. 19th European photovoltaic PVSEC-19, Paris France,1497-1500, (**2004**).
[2] A. Chovet P. Masson,
"Physique des semi-conducteurs'' Ecole polytechnique universitaire de marseille departement micro-electronique et telecommunications, p.11.
[3] S.K.Khadka,
"Semiconductor diode, theory and principles", Nepal (**2018**).
[4] "semiconductors applied physics", p.1.
[5] R.Karan,
"Difference Between Intrinsic and Extrinsic Semiconductors", (**2023**).
[6] P.S.Aithal,
"Basic electronics'', New Delhi, p 3-5, (**2011**).
[7] "Semiconductor electronics: materials, devices and simple circuits", p 333-334.
[8] "Semiconductor diode".
[9] "Introduction to semiconductors", p.1.
[10] A.Rahman,
"A Review on Semiconductors Including Applications and Temperature Effects in Semiconductors", American scientific research journal for engineering, technology, and sciences (ASRJETS), volume 7, No 1, p.62, (**2014**).
[11] M.Ashraf,
"Non-Renewable Energy Resources".
[12] "Energy efficiency and renewable energy", p.1, (**2001**).
[13] K.Nada,
"Renewable Energy Types", Journal of Clean Energy Technologies, Vol. 2, No. 1, p.1, (**2014**).

[14] M.Iqbal,
"An introduction to solar radiation", department of mechanical engineering the university of British Columbia Vancouver, p 1-3, (**1984**).
[15] C.J.Chen,
"Physics of Solar Energy", department of applied physics and applied mathematics columbia university, p.109, (**2011**).
[16] P.J.Tyson,
"Climate change earth-sun relationships", p.3, (**2006**).
[17] A.E.Dixon, J.D.Leslie,
"Solar energy conversion", department of physics, university of waterloo, Ontario, Canada, p.3, (**1978**).
[18] J.Wid, J.Munkhammar,
"Solar radiation theory", department of engineering sciences, uppsala university, p 17-19, (**2019**).
[19] "Chapter 7 measurement of sunshine duration and solar radiation", p 6-8.
[20] B.Zaidi,
"Introduction to Photovoltaic Effect", p.1, (**2018**).
[21] J.L.Gray,
"The physics of the solar cell", Purdue University, West Lafayette, Indiana, USA, p.83, (**2011**).
[22] T.Dittrich,
"Materials concepts for solar cells", p 8-10, (**2015**).
[23] R.Swami,
"Solar cell", Lecturer, department of electronics, Chhattisgarh, India International Journal of Scientific and Research Publications, Volume 2, Issue 7, p 2-3, (**2012**).
[24] A.H.M.Smets, K.Jäger, O.Isabella, R.Swaaij, M.Zeman,
"Solar energy the physics and engineering of photovoltaic conversion, technologies and systems", England, p.261.
[25] R.Nazar,
"Improvement of efficiency of solar panel using different methods", international journal of electrical and electronics engineers, volume 07, issue 01, department of Electrical and Electronics., Lingaya's University, Faridabad, India, p 13-15, (**2015**).

[26] A.goetzberger, J.knobloch,
“Crystalline Silicon Solar Cells”, Vo13 Fraunhofer Institute for solar energy systems, Freiburg, Germany, p.115, (**1998**).

[27] G.T.Chavan,
“A Brief Review of Transparent Conducting Oxides (TCO): The Influence of Different Deposition Techniques on the Efficiency of Solar Cells”, p.2, (**2023**).

[28] R.A.Afre, N.Sharma, M.Sharon,
“Transparent conducting oxide films for various applications”, walchand center for research in nanotechnology and bionanotechnolog, W-H Marg, Ashok Chowk, Solapur, Maharashtra, India, p 80-81, (**2017**).

[29] M.Axelsson,
“Transparent conductive oxides deposited by magnetron sputtering: synthesis and characterization”, Sweden, p.2, (**2019**).

[30] J.Barksdale,
“Titanium, Its Occurrence”, Chemistry, and Technology, 2nd Edition, Roland Press Company, New York (**1966**).

[31] K. G. Budinski,
"Surface Engineering for Wear Resistance. (Retroactive Coverage)." Prentice-Hall, Inc, Englewood Cliffs, New Jersey 07632, United States, 1988. 420 (**1988**).

[32] M. J. Gázquez, J. P. Bolivar, R. Garcia-Tenorio, F. Vaca,
"A review of the production cycle of titanium dioxide pigment." Materials Sciences and Applications 5 (07), 441-458, (**2014**).

[33] A. Pottier, S.Cassaignon, C. Chanéac., F. Vilain., E. Tronc, J.P. Jolivet,
“Size tailoring of TiO2 anatase nanoparticles in aqueous medium and synthesis of nanocomposites. Characterization by Raman spectroscopy”, Journal of Materials Chemistry 13, 877 (**2003**).

[34] T.Hitosugi,
“TiO2-based Transparent Conducting Oxide”, Advanced Institute for Materials Research (WPI-AIMR), Tohoku University, p.2.

[35] B. Thomas,
"Des nanotitanates de soduim aux dioxydes de titane : électrode négative à base de TiO_2 (B) nanométrique pour accumulateur lithium ion”, Thèse de Doctorat, Université de Nantes, France (**2009**).

[36] S. Pardis,
"Synthèse de nanoparticules d'oxyde de titane par pyrolyse laser : étude des propriétés optiques et de la structure électronique", Thèse de Doctorat, Université Paris Sud XI, France (**2001**).
[37] B. S. Richards,
"Novel uses of titanuim dioxide for silicon solar cells", Thèse de Doctorat, Université de New South Wales Sydney2052, Australie, (**2002**).
[38] J. Schneider, M. Matsuoka, M. Takeuchi, J. Zhang, Y. Horiuchi, M. Anpo, D.W. Bahnemann,
"Understanding TiO_2 Photocatalysis: Mechanisms and Materials", Chem. Rev. 114 (19), 9919-9986, (**2014**).
[39] S. D. Mo, W. Y. Ching,
"Electronic and optical properties of three phases of titanium dioxide: Rutile, anatase, and brookite", Physical review B, 51 (1), (**1995**).
[40] N.Besseghir, I.Bennour,
"Optimisation par simulation d'une cellule solaire à Hétérojonction'', mémoire de master, p.87.
[41] A.Djafour,
"Etude et simulation d'une cellule solaire à hétérojonction de type ZnO/n-Si"
Mémoire de master, p.66.
[42] Https://www.researchgate.net/figure/Energy-band-diagram-for-a-metal-semiconductor-n-type-contact-in-the-case-PH-m-PH-s_fig2_255700954, 10/05/2024, 18:20.
[43] C.Yadav,
"Numerical simulation for optimization of ultra-thin n-type AZO and TiO2 based textured p-type c-Si Heterojunction Solar Cells", (**2021**).
[44] "Etude de l'oxyde de titane en couches minces en hétérojonction avec le silicium, application photovoltaïque".
Memoire de magister, p.58.
[45] M.Manoua, T.Jannane, O.Abouelala, M.Sajieddine, M.Mabrouki,A.Almaggoussi,A.Liba,
"Optimization of ZnO thickness for high efficiency of n-ZnO/p-Si heterojunction solar cells by 2D numerical simulation", (**2020**).
[46] Z.Toufik, Lidjici Hamza, Zoukel Abdelhalim, Mahrane Achour,
"Comparative Numerical Simulation Between p and n-type Substrate of Heterojunction with Intrinsic Silicon Solar Cell", Unité de Développement des Equipements Solaire. UDES/Centre de Développement des Energies Renouvelable, Bou Ismail, Tipaza, Algérie, (**2019**).

الملخص

يتم تحويل الطاقة الشمسية الى طاقة كهربائية من خلال استخدام الخلايا الكهروضوئية والتي تأتي ببنيات مختلفة بهدف الحصول على أفضل أداء.

تطرقنا في هذا البحث لدراسة الخلايا الشمسية غير المتجانسة وقمنا باستخدام برنامج المحاكاة الرقمية Afors-het

لمحاكاة خليتين غير متجانستين والمتمثلتين في TiO_2(n)-c-Si(p) و ZnO(n)-c-Si(p)

ثم قمنا بعد ذلك بدراسة تأثير تغيرات التطعيم في كل من السليكون والأكاسيد الموصلة الشفافة والمتمثلة في ثنائي أكسيد التيتانيوم وأكسيد الزنك وكذا تغيرات سمك طبقة السيلكون وسمك الاكاسيد الموصلة الشفافة على أداء الخلية الشمسية وهذا بتحديد القيم التالية: كفاءة الخلية، عامل التعبئة، كثافة تيار الدارة القصيرة وجهد الدارة المفتوحة.

أظهرت النتائج التي تحصلنا عليها أن هذا النوع من الخلايا بإمكانه تحقيق أفضل كفاءة بنسبة 21,23% عند ثنائي أكسيد التيتانيوم ونسبة 21,05% عند أكسيد الزنك.

الكلمات المفتاحية: برنامج المحاكاة الرقمية Afors-het ، خليتان غير متجانستان TiO_2(n)-c-Si(p)وZnO(n)-c-Si(p)، كفاءة الخلية، عامل التعبئة، كثافة تيار الدارة القصيرة وجهد الدارة المفتوحة.

RESUME

L'énergie solaire est convertie en énergie électrique grâce à l'utilisation de cellules photovoltaïques, qui sont disponibles en plusieurs configurations pour maximiser leur efficacité.

Dans cette mémoire, nous étudions les cellules solaires à hétérojonction en utilisant le logiciel de simulation numérique Afors-het (Automate for simulation of hétérostructures). On utilise ce logiciel pour simuler les cellules solaires à hétérojonction TiO_2(n)-c-Si(p) et ZnO(n)-c-Si(p).

On fait ça pour examiner les effets de la variation des épaisseurs et la variation du dopage de silicium et de TCOs représentés par TiO_2 et ZnO, sur les performances des cellules :le rendement η, le facteur de forme FF , la densités de courant de court-circuit J_{SC} , la tension de circuit ouvert V_{OC} .

Les résultats obtenus nous montrent que ces formes de cellules solaires peuvent atteindre un rendement supérieur de 21,23% avec TiO_2 et 21,05% avec ZnO.

Mot clés : Afors-het, hétérostructures, les cellules solaires TiO_2(n)-c-Si(p) et ZnO(n)-c-Si(p), le rendement η , le facteur de forme FF , la densité de courant de court-circuit J_{SC} et la tension de circuit ouvert V_{OC} .

ABSTRACT

Solar energy is converted into electrical power through the use of photovoltaic cells, which come in a variety of configurations to maximise their efficiency.

Using the numerical simulation programme Afors-het (Automate for simulation of heterostructures), we study heterojunction solar cells in this memory. We use it to simulate the TiO_2(n)-Si(p) and the ZnO(n)-Si(p) heterojunction solar cells. With this simulation, we examine the effects of varying silicon and TCOs represented by ZnO and TiO_2 doping and the influence of TCOs and silicon thicknesses on the cells performance, particularly: the efficiency η, fill factor FF, short-circuit voltage J_{SC}, open circuit voltage V_{OC}.

The obtained results demonstrate that these forms of solar cells can attain a superior efficiency of 21.23% with TiO_2 and 21.05% with ZnO.

Key words: Afors-het , heterostructure, TiO_2(n)-c-Si(p) and ZnO(n)-c-Si(p) solar cells, efficiency η , fill factor FF ,short-circuit voltage J_{SC} and open circuit voltage V_{OC}.